

# Spin Structure of the Proton and Large $p_T$ Processes in Polarized $pp$ Collisions

L. E. Gordon<sup>a,b\*</sup> and G. P. Ramsey<sup>c,d†</sup>

<sup>a</sup> *Theory Group, Jefferson Lab, Newport News, VA 23606*

<sup>b</sup> *Hampton University, Hampton, VA 23606*

<sup>c</sup> *High Energy Physics Division, Argonne National Laboratory, Argonne, IL 60439, USA*

<sup>d</sup> *Loyola University, Chicago, IL 60626*

## Abstract

QCD motivated polarized parton distributions, evolved directly in  $x$ -space, are used to predict rates for prompt photon and Jet production at RHIC and HERA- $\vec{N}$  center of mass energies. Various scenarios for the polarized gluon distributions are considered and compared, and the possibility of using large  $p_T$  processes in polarized  $pp$  collision experiments to choose between them is analyzed.

Typeset using REVTeX

---

\*E-mail address: lgordon@cebaf.gov

†Work supported in part by the U.S. Department of Energy, Division of High Energy Physics, Contract W-31-109-ENG-38. E-mail address: gpr@hep.anl.gov

## I. INTRODUCTION

Interest in spin physics has grown in the last few years thanks to the various polarized DIS experiments and to existing proposals for future polarized beam experiments. One proposal includes the construction of a polarized  $ep$  collider at DESY (HERA- $\vec{N}$ ) running at an energy of  $\approx 40$  GeV, which will complement and extend the results to be obtained at the Relativistic Heavy Ion Collider (RHIC) at Brookhaven. Polarized deep-inelastic scattering experiments have shed light on the relative contributions of the nucleon constituents to their overall spin. However, the largest theoretical uncertainties are from: (1) the polarized gluon size and shape as a function of  $x$  being unknown and (2) the relative size of the polarized sea distributions being uncertain. [1]

In a recent paper, [2] we proposed three new parametrizations for the spin dependent parton distributions for the proton. Our distributions, which are available in both leading order (LO) and next-to-leading order (NLO), were evolved directly in  $x$ -space. In ref. [2] we presented details of the models used to obtain the input distributions and compared the evolved structure functions with the available data. All currently available data on the nucleon spin structure come from deep inelastic scattering experiments, and therefore do not contain direct information on individual parton distributions such as the gluon,  $\Delta G(x, Q^2)$  or strange sea,  $\Delta s(x, Q^2)$ , for example. It is expected that such detailed information will come from other experiments such as those proposed at RHIC and HERA- $\vec{N}$ .

As a  $pp$  collider, RHIC will be endowed with a very high integrated luminosity (up to 800  $\text{pb}^{-1}$  at 500 GeV) and will be spanning a center of mass energy range between 50 to 500 GeV. One of the main programs at RHIC will be to determine the size and shape of the polarized parton distributions which, at the moment, suffer from significant model dependence. There are large uncertainties in both the gluon contribution,  $\Delta G$ , and the sea quark distributions.

In this paper we continue the work of ref. [2] by providing details of the  $x$ -space evolution of the parton distributions. We also compare our evolved distributions with another parametrization in order to highlight the similarities and differences between them. Finally, we use our evolved parton distributions to predict cross sections and asymmetries for direct photon and single jet production at RHIC and HERA- $\vec{N}$  energies.

## II. INPUT DISTRIBUTIONS

In reference [2], we constructed three sets of polarized parton distributions for the valence and all light sea flavors of quarks. Each set corresponds to a particular model of the polarized gluons, motivated by different physical assumptions. All of the  $x$ -dependent polarized quark distributions are generated from the unpolarized distributions [3] and some basic theoretical assumptions. The valence up and down distributions are generated from a broken SU(6) model of the polarized valence quarks. For the sea distributions, we built in positivity constraints and incorporated the integrated and  $x$ -dependent polarized deep-inelastic scattering data. The three models of the polarized gluons used to generate the distributions are assumed small at the relatively low  $Q^2$  values of the data. One model gives a positively polarized gluon, generated from the unpolarized glue: ( $\Delta G = xG$ ), one is an unpolarized gluon ( $\Delta G = 0$ ), and the third is based upon an instanton model, which

integrates to a slightly negative value. All three sets of distributions are in good agreement with the data, an indication that the polarized distributions are still not well determined.

All of our distributions are generated at  $Q_0^2 = 1.0 \text{ GeV}^2$  and are evolved up to the  $Q^2$  values necessary for predicting the appropriate spin observables. Evolution for the singlet and non-singlet functions is done in  $x$ -space to the NLO level. We have assumed three quark flavors up to the appropriate  $Q^2$  value for charm production, whereby we smoothly introduce the fourth flavor to the evolution equations. Details will be discussed briefly in the next section.

The distributions we use here are strongly embedded in sound theoretical assumptions, while giving good agreement with all of the latest polarized DIS data. In order to determine the nature of the polarized distributions to a finer degree of detail, we are using them to generate predictions of the spin asymmetries for direct photon and jet production. These processes are feasible for the RHIC and HERA experimental groups and there is general agreement that they are pivotal in helping to determine the nature of the polarized gluon distribution.

### III. $X$ -SPACE EVOLUTION IN LEADING AND NEXT-TO-LEADING ORDER

Given the polarized parton distributions at some reference scale  $Q_0^2$ , they can be predicted at a higher scale  $Q^2$  by solving the polarized DGLAP evolution equations. For the non-singlet sector the evolution equation is given by

$$\frac{d\Delta q_{NS}(x, Q^2)}{d \ln Q^2} = \frac{\alpha_s(Q^2)}{2\pi} \Delta P_{NS}^\pm(x) * \Delta q_{NS}(x, Q^2), \quad (3.1)$$

where  $\Delta q_{NS}(x, Q^2)$  is the polarized non-singlet parton distribution function,  $\Delta P_{NS}^\pm(x)$  are polarized non-singlet splitting functions,  $\alpha_s(Q^2)$  is the strong coupling constant and  $*$  represents the convolution

$$f(x) * g(x) = \int_x^1 \frac{dy}{y} f\left(\frac{x}{y}\right) g(y). \quad (3.2)$$

For the polarized singlet sector, with the quark singlet defined by

$$\Delta \Sigma = \sum_i (\Delta q_i + \Delta \bar{q}_i), \quad (3.3)$$

the evolution equations are

$$\begin{aligned} \frac{d\Delta \Sigma(x, Q^2)}{d \ln Q^2} &= \frac{\alpha_s(Q^2)}{2\pi} \left[ \Delta P_{qq}(x) * \Delta \Sigma(x, Q^2) + \Delta P_{qg}(x) * \Delta G(x, Q^2) \right] \\ \frac{d\Delta G(x, Q^2)}{d \ln Q^2} &= \frac{\alpha_s(Q^2)}{2\pi} \left[ \Delta P_{gq}(x) * \Delta \Sigma(x, Q^2) + \Delta P_{gg}(x) * \Delta G(x, Q^2) \right]. \end{aligned} \quad (3.4)$$

The splitting functions have the perturbative expansion

$$\Delta P_{ij}(x) = \Delta P_{ij}^{(0)}(x) + \frac{\alpha_s(Q^2)}{2\pi} \Delta P_{ij}^{(1)}(x) + \dots \quad (3.5)$$

The first term is the leading order (LO) contribution and the second term the next-to-leading order (NLO) contribution to the splitting kernels, which were calculated in ref. [4]. In leading order we use the expression

$$\alpha_s(Q^2) = \frac{4\pi}{\beta_0 \ln(Q^2/\Lambda^2)}, \quad (3.6)$$

and in NLO

$$\alpha_s(Q^2) = \frac{4\pi}{\beta_0 \ln(Q^2/\Lambda^2)} \left[ 1 - \frac{\beta_1 \ln \ln(Q^2/\Lambda^2)}{\beta_0^2 \ln(Q^2/\Lambda^2)} \right] \quad (3.7)$$

for the strong coupling constant. The constants  $\beta_0$  and  $\beta_1$  are defined by

$$\beta_0 = \frac{11}{3}N_c - \frac{2}{3}N_f, \quad \beta_1 = \frac{34}{3}N_c^2 - \frac{10}{3}N_cN_f - 2C_F N_f, \quad (3.8)$$

with the color constants  $N_c = 3$  and  $C_F = 4/3$ , and  $N_f$  is the number of active quark flavors.

In order to solve the DGLAP evolution equations directly in  $x$ -space we use the ansatz proposed in ref. [5]. We assume a solution of the form

$$\Delta q(x, Q^2) = \sum_{n=0}^{\infty} \frac{A_n(x)}{n!} \ln^n \left( \frac{\alpha_s(Q^2)}{\alpha_s(Q_0^2)} \right) + \alpha_s(Q^2) \sum_{n=0}^{\infty} \frac{B_n(x)}{n!} \ln^n \left( \frac{\alpha_s(Q^2)}{\alpha_s(Q_0^2)} \right), \quad (3.9)$$

where  $\Delta q = (\Delta q_{NS}, \Delta \Sigma, \Delta G)$ . Since the sum starts at  $n = 0$ , boundary conditions,  $q(x, Q_0^2) = q_0(x)$ , can be incorporated into the equations. When Eq. (3.9) is inserted into the DGLAP equations and all third-order terms are dropped, the relations

$$\begin{aligned} A_0(x) &= q_0(x) \\ B_0(x) &= 0 \\ A_{n+1}(x) &= -\frac{2}{\beta_0} P^{(0)}(x) * A_n(x) \\ B_{n+1}(x) &= (-\delta(1-x) - \frac{2}{\beta_0} P^{(0)}(x)) * B_n(x) - \frac{1}{\pi\beta_0} P^{(1)}(x) * A_n(x) - \frac{\beta_1}{4\pi\beta_0} A_{n+1}(x) \end{aligned} \quad (3.10)$$

are obtained for the  $A_n(x)$  and  $B_n(x)$ . The functions  $P^{(0,1)}(x)$  are the LO and NLO parts of the splitting functions, while the terms  $A_n(x)$  and  $B_n(x)$  represent the LO and NLO coefficients respectively. If a LO evolution is desired then only the  $A_n(x)$  are calculated and the LO expression for  $\alpha_s$  is used. These equations can be solved numerically for any value of  $x$ , and the coefficients substituted into Eq. (3.9) to obtain the distributions  $\Delta q(x, Q^2)$  at any value of  $Q^2$ . Details of the input distributions and expressions for the coefficients are given in the Appendix.

## IV. LARGE $P_T$ PROCESSES AT RHIC AND HERA- $\vec{N}$

### A. Experimental Parameters

The polarization experiments planned for RHIC show great promise for the high energy community. With polarized proton beams of 70% polarization and a planned luminosity of

$\mathcal{L} = 2 \times 10^{32}/\text{cm}^{-2}/\text{sec}^{-1}$ , both direct- $\gamma$  production and jet production can be done in a kinematic region where we can gain tremendous insight into the polarized gluon distribution. These are part of the planned set of experiments for both the STAR and PHENIX detectors at RHIC. [6] If the experiments are able to obtain an integrated luminosity, presently assumed to be  $320 \text{ pb}^{-1}$  at  $\sqrt{s} = 200 \text{ GeV}$  and  $800 \text{ pb}^{-1}$  at  $\sqrt{s} = 500 \text{ GeV}$ , the resulting data should be enough to distinguish between various polarized gluon models which have been proposed. [2,7]

The STAR detector will have a wide angular coverage to cover a large kinematic region for Jet production. Their range of  $x$  will extend from about  $0.02 \leq x \leq 0.30$  ( $\pm 0.02$ ) with an approximate uncertainty of  $\delta\langle\Delta G\rangle \approx \pm 0.05$ .

The PHENIX detector will measure high  $p_T$  prompt  $\gamma$ 's in the kinematic range of  $10 \leq p_T \leq 30 \text{ GeV}$  at  $\sqrt{s} = 200 \text{ GeV}$  ( $x \leq 0.25$ ) and  $10 \leq p_T \leq 40 \text{ GeV}$  at  $\sqrt{s} = 500 \text{ GeV}$  ( $x \leq 0.15$ ). The angular coverage is not as large as STAR but it has finer granularity. The estimated uncertainty is  $\delta\langle\frac{\Delta G}{G}\rangle \approx \pm 0.05 \rightarrow 0.30$ , increasing linearly with  $p_T$ . The combination of the two detectors will be valuable in covering a wide kinematic range with reasonable error bars for cross sections and asymmetries.

Tests are presently being performed to polarize the proton beam at HERA. The success of these tests will provide a unique kinematic region for measuring asymmetries in direct  $\gamma$  and Jet production. [8] These experiments will be performed at  $\sqrt{s} = 40 \text{ GeV}$ , giving a good sensitivity to distinguishing between gluon model predictions for the corresponding asymmetries. This will be discussed later.

All of the above mentioned experimental groups plan to measure the observables in both direct- $\gamma$  and Jet production. Present plans call for the RHIC experiments to be performed in the next five years, while the HERA experiments would hopefully follow shortly thereafter. Both sets of experiments are important, as the lower center-of-mass energies appear to be somewhat better for distinguishing the size of the polarized gluons. Thus, the combination of a wide kinematic range and reasonable uncertainties should give a good indication of the size and shape of the polarized gluon distribution.

## B. Theoretical Background

### 1. Prompt Photon Production

The prompt photon cross section promises to be one of the most useful for measuring  $\Delta G$  at RHIC and HERA- $\vec{N}$  since it is dominated by initial  $qg$  scattering. Contributions to the prompt photon cross section are usually separated into two classes in both LO [9] and NLO. [10–12] There are the so-called direct processes,  $ab \rightarrow \gamma c$  in LO and  $ab \rightarrow \gamma cd$ , in NLO,  $a, b, c$  and  $d$  referring to partons, where the photon is produced directly in the hard scattering. In addition there are the fragmentation contributions where the photon is produced via bremsstrahlung off a final state quark or gluon,  $ab \rightarrow cd(e)$  followed by  $c \rightarrow \gamma + X$  for instance.

In LO,  $O(\alpha\alpha_s)$ , the direct subprocesses contributing to the cross section are

$$\begin{aligned} qg &\rightarrow \gamma q \\ q\bar{q} &\rightarrow \gamma g. \end{aligned} \tag{4.1}$$

In addition there are the fragmentation processes

$$\begin{aligned}
qg &\rightarrow qg \\
qq &\rightarrow qq \\
qq' &\rightarrow qq' \\
q\bar{q} &\rightarrow q\bar{q} \\
qg &\rightarrow qg \\
q\bar{q} &\rightarrow gg \\
gg &\rightarrow gg \\
gg &\rightarrow q\bar{q}
\end{aligned} \tag{4.2}$$

where one of the final state partons fragments to produce the photon, *i.e.*,  $q(g) \rightarrow \gamma + X$ .

In the direct processes in LO, the differential cross section is given by

$$E_\gamma \frac{d\Delta\sigma_{dir}^{LO}}{d^3p_\gamma} = \frac{1}{\pi S} \sum_{i,j} \int_{VW}^V \frac{dv}{1-v} \int_{VW/v}^1 \Delta f_1^i(x_1, M^2) \Delta f_2^j(x_2, M^2) \frac{1}{v} \frac{d\Delta\hat{\sigma}_{ij\rightarrow\gamma}}{dv} \delta(1-w) \tag{4.3}$$

where  $S = (P_1 + P_2)^2$ ,  $V = 1 + T/S$ ,  $W = -U/(T + S)$ ,  $v = 1 + \hat{t}/\hat{s}$ ,  $w = -\hat{u}/(\hat{t} + \hat{s})$ ,  $\hat{s} = x_1 x_2 S$ , and  $T = (P_1 - P_\gamma)^2$  and  $U = (P_2 - P_\gamma)^2$ . As usual the Mandelstam variables are defined in the upper case for the hadron-hadron system and in lower case in the parton-parton system.  $P_1$  and  $P_2$  are the momenta of the incoming hadrons and  $\Delta f_1^i(x_1, M^2)$  and  $\Delta f_2^j(x_2, M^2)$  represent the respective probabilities of finding parton  $i$  and  $j$  in hadrons 1 and 2 with momentum fractions  $x_1$  and  $x_2$  at scale  $M^2$ . The quantity  $d\Delta\hat{\sigma}_{ij\rightarrow\gamma}/dv$  is the hard subprocess cross section which is calculable in perturbative QCD.

For the fragmentation processes, the differential cross section is given by

$$\begin{aligned}
E_\gamma \frac{d\Delta\sigma_{frag}^{incl}}{d^3p_\gamma} &= \frac{1}{\pi S} \sum_{i,j,l} \int_{1-V+VW}^1 \frac{dz}{z^2} \int_{VW/z}^{1-(1-V)/z} \frac{dv}{1-v} \int_{VW/vz}^1 \frac{dw}{w} \Delta f_1^i(x_1, M^2) \Delta f_2^j(x_2, M^2) \\
&\times \frac{1}{v} \frac{d\Delta\hat{\sigma}_{ij\rightarrow l}}{dv} \delta(1-w) D_{\gamma/l}(z, M_f^2),
\end{aligned} \tag{4.4}$$

where  $D_{\gamma/l}(z, M_f^2)$  represents the probability that the parton labelled  $l$  fragments to a photon with a momentum fraction  $z$  of its own momentum at scale  $M_f^2$  (note that  $D_{\gamma/l}(z, M_f^2)$  is the usual unpolarized fragmentation function, since the final state is not polarized). This is the non-perturbative fragmentation function which must be obtained from experiment at some scale and evolved to  $M_f^2$  using the usual evolution equations.

In NLO,  $O(\alpha_s^2)$ , there are virtual corrections to the LO non-fragmentation processes of Eq. (4.1), as well as the further three-body processes:

$$g + q \rightarrow g + q + \gamma \tag{4.5a}$$

$$g + g \rightarrow q + \bar{q} + \gamma \tag{4.5b}$$

$$q + \bar{q} \rightarrow g + g + \gamma \tag{4.5c}$$

$$q + q \rightarrow q + q + \gamma \tag{4.5d}$$

$$\bar{q} + q \rightarrow \bar{q} + q + \gamma \tag{4.5e}$$

$$q + \bar{q} \rightarrow q' + \bar{q}' + \gamma \tag{4.5f}$$

$$q + q' \rightarrow q + q' + \gamma. \tag{4.5g}$$

In principle the the fragmentation processes of Eq. (4.2) should now be calculated to  $O(\alpha_s^3)$  and convoluted with the NLO photon fragmentation functions whose leading behaviour is  $O(\alpha/\alpha_s)$ , but they have not yet been calculated for the polarized case, hence, in both the polarized and unpolarized cases, we include the leading order contributions to these processes only.

The direct contribution to the inclusive cross section is given by

$$E_\gamma \frac{d\Delta\sigma_{dir}^{incl}}{d^3p_\gamma} = \frac{1}{\pi S} \sum_{i,j} \int_{VW}^V \frac{dv}{1-v} \int_{VW/v}^1 \frac{dw}{w} \Delta f_1^i(x_1, M^2) \Delta f_2^j(x_2, M^2) \times \left[ \frac{1}{v} \frac{d\Delta\hat{\sigma}_{ij\rightarrow\gamma}}{dv} \delta(1-w) + \frac{\alpha_s(\mu^2)}{2\pi} \Delta K_{ij\rightarrow\gamma}(\hat{s}, v, w, \mu^2, M^2, M_f^2) \right], \quad (4.6)$$

where  $\Delta K_{ij\rightarrow\gamma}(\hat{s}, v, w, \mu^2, M^2, M_f^2)$  represents the higher corrections to the hard subprocess cross sections calculated in [11] and  $\mu$  is the renormalization scale.

In this paper we present results for the inclusive prompt photon cross section without taking any possible isolation cuts into account. As shown in ref. [12], isolation cuts do not have a significant effect on the asymmetries, which are the quantities in which we are mainly interested here. It is also unlikely that isolation will be necessary at HERA cms energies.

## 2. Single Jet Production

We calculate the single jet cross section at LO only. In this case the approximation ‘parton = jet’ is used and a jet definition is not needed. The eight subprocesses listed in Eq. (4.2) are the same ones contributing to jet production in LO. The differential cross section is given by;

$$E_J \frac{d\Delta\sigma^J}{d^3p_J} = \frac{1}{\pi S} \sum_{i,j} \int_{VW}^V \frac{dv}{1-v} \int_{VW/v}^1 \Delta f_1^i(x_1, M^2) \Delta f_2^j(x_2, M^2) \frac{1}{v} \frac{d\Delta\hat{\sigma}_{ij\rightarrow J}}{dv} \delta(1-w) \quad (4.7)$$

where the variables are defined as before. [13] Recently the polarized jet cross section has been calculated in NLO, [14] but for the purposes of this paper we use the leading order calculation.

## C. Significance of Results

We now compare our three sets of polarized distributions, (GGRA, GGRB and GGRC) [2] generated from the three gluon models discussed in section II, with those of Gehrmann and Stirling, [15] set GSA. Our polarized gluon distributions are smaller than those of GSA, which affects the ratio of quark to gluon contributions at small  $x$ . This in turn will modify the relative contributions to direct- $\gamma$  production and Jet production. (See fig. 1a). The polarized sea peaks at higher  $x$  and goes negative at much larger  $x$  than the GSA distributions, which will further affect the relative contributions at small  $x$ . (See figs. 1b and 1c). Our valence distributions are also larger, which makes the qq contributions to both processes larger. (See fig. 1d). For GGRA, the LO and NLO distributions are similar,

implying perturbative stability. The result is similar for GGRB and GGRC (figs. 1c and 1d).

The comparative results for direct- $\gamma$  production are shown in figures 2 through 4. At  $\sqrt{S} = 200$  GeV, the cross section is measurable out to  $p_T \sim 40 - 50$  GeV, given the planned luminosities of RHIC (fig. 2a). The  $A_{LL}^\gamma$  asymmetry in direct- $\gamma$  production differs significantly from GSA only at the largest  $p_T$  values ( $> 40$  GeV), where the PHENIX detector at RHIC is at an upper  $p_T$  limit. However, expected errors in the measurement of the asymmetry,  $A_{LL}^\gamma$ , at PHENIX are much smaller at the lower  $p_T$  values. [16] Up to  $p_T$  of about 15 GeV, the expected error is about  $\pm 0.006$  and grows to about  $\pm 0.080$  at 30 GeV. Thus, measurement of this asymmetry should be done at all possible  $p_T$  values, with those at lower  $p_T$  possibly able to distinguish between the small and large polarized gluon distributions, despite their close proximity. (See fig. 2b). At  $\sqrt{S} = 200$  GeV, the  $qg$  processes in GGRA dominate (positive  $\Delta G$ ) much more than the GSA and our other gluon models, which give the larger  $A_{LL}^\gamma$  values seen at larger  $p_T$ . The  $q\bar{q}$  contributions are relatively small at all  $p_T$  for all models. See fig. 2c for details. Thus, the  $qg$  processes dominate, as expected. In fig. 3a, we plot the direct- $\gamma$  cross section as a function of rapidity,  $y^\gamma$  at  $p_T^\gamma = 15$  GeV. The cross section remains of reasonable size out to rapidities past  $|y^\gamma| \approx 1.3$ . The corresponding asymmetries (fig. 3b) are relatively flat out to  $|y^\gamma| \approx 1$ , after which they exhibit a slight rise. They become quite large at rapidities which are out of the range for PHENIX, but possibly accessible by the endcap of the STAR detector. It may be advantageous to take measurements at  $|y^\gamma| \geq 1$  at the appropriate ranges of rapidity with both detectors for better sensitivity to the asymmetries.

At HERA energies,  $\sqrt{s} \approx 40$  GeV, the cross section is reasonable for ranges of  $p_T$  up to about 10 GeV (fig. 4a). There are differences in the asymmetry  $A_{LL}^\gamma$ , which depend upon the models of the polarized distributions. However, these differences manifest themselves more greatly at  $p_T \approx 10$  GeV and above. The sizes of  $A_{LL}^\gamma$  are still large enough at the planned  $p_T$  values at HERA (about 2  $\rightarrow$  8 GeV) to be measured. Since the asymmetries diverge quicker at the HERA center-of-mass energy than at higher  $\sqrt{s}$ , there may be a good chance that a more precise determination of the polarized gluon can be made. A lot depends upon the relative errors expected from such measurements at each  $p_T^\gamma$ . (See fig. 4b). Thus, even the moderately sized positive  $\Delta G$  gives a relatively large asymmetry,  $A_{LL}^\gamma$ . Small asymmetries would indicate a very small, if not negative  $\Delta G$  in this kinematic region. A possible problem exists, since the expected experimental errors tend to increase substantially with increasing  $p_T$ . Thus, these two cases may not be distinguishable. It is recommended that  $A_{LL}^\gamma$  be measured over a wide range of  $p_T$ , up to the largest values possible, to test the consistency of these models.

Although the direct- $\gamma$  cross sections are significantly larger at the RHIC energy of  $\sqrt{S} = 500$  GeV, the asymmetries are correspondingly smaller and it would be much more difficult to determine the polarized gluon distribution from direct- $\gamma$  production. Thus, we highly recommend that these measurements be done at HERA- $\vec{N}$  and at the lower  $\sqrt{S}$  values at RHIC.

Figures 5 through 6 show our predictions for jet production ( $pp \rightarrow \text{Jet}+X$ ) using these distributions. The cross sections are measurable for all the planned values of  $p_T^J$ . These are shown for zero rapidity at  $\sqrt{S} = 200$  GeV in fig. 5a. The  $q\bar{q}$  and  $qg$  processes both dominate in our model for  $A_{LL}^J$  at large  $p_T^J$ . The  $qg$  is more dominant at smaller  $p_T^J$ , with comparable



contributions at the limit of the RHIC STAR detector, ( $p_T \approx 25$  GeV at  $\sqrt{S} = 200$  GeV). This is consistent with the discussion above. The GSA model has the  $qg$  process totally dominant with  $qg$  small (see fig. 5b). However, their asymmetries are quite a bit smaller than ours for  $p_T^J \geq 20$  GeV and ours rise with  $p_T^J$ , while theirs remain constant. A measurement of  $A_{LL}^J$  for different  $p_T^J$  at the smaller  $\sqrt{S}$  region of RHIC may be able to distinguish among these models, and give an indication as to which process does indeed dominate in this kinematical region. The GS and GGR models are both around the 4  $\rightarrow$  6% level at  $p_T^J \approx 20$  GeV while the GGR asymmetries grow with  $p_T^J$  up to the maximum values at RHIC (see fig. 5c). Our asymmetries for the other gluon models exhibit the same  $p_T^J$  behavior, except that the values are smaller (up to about the 10% level at the limit). Again, it is important that the errors in jet measurement at STAR be minimized, in order to distinguish among the models at these levels. This can be, at least in part, accomplished with the endcap installed, which will provide enhanced jet coverage in this kinematic region. Distinguishing among the various models can yield vital information about both the polarized gluons and quark distributions in Jet production. (See figs. 5d and 5e).

At large  $\sqrt{s} \approx 500$  GeV, the cross sections are larger than at 200 GeV (see fig. 6a), but the corresponding asymmetries in Jet production are much smaller and cannot distinguish between the various models, (fig. 6b) even at the largest  $p_T^J$  values available. Thus, it is recommended that these asymmetries be measured at the lower center-of-mass energies.

## V. DISCUSSION

We have calculated the cross sections and asymmetries for polarized direct- $\gamma$  production and Jet production at RHIC and HERA (for  $\gamma$  production) cms energies, using the polarized distributions generated in reference [2]. Comparisons of our predictions with those of other distributions were discussed in light of the physics that can be extracted from performing these experiments. The entire  $Q^2$  evolution for these predictions was done for LO and NLO in  $x$ -space using a technique explained in the text and in the Appendix. This gives highly reliable results without the use of moments. Both the LO and NLO evolution programs are written in FORTRAN and are available from either author via electronic mail.

We have shown that if the polarized gluon distribution is even moderately positive at  $Q^2 = 1$  GeV, the asymmetry for direct photon production is among the best candidates for determining the size of  $\Delta G$ . The size of the predicted asymmetries may, however, be less relevant if the experimental errors are too large. Jet production is a close contender for determining which models of  $\Delta G$  give the best agreement with data. Much will depend upon the relative errors in the applicable kinematic regions for PHENIX (photon detection) and STAR (detection of photons/jets). For details, see the articles by Y. Goto, S. Vigdor, S. Hoppelman and D. Underwood in ref. [6] At this point, it appears that the projected errors for direct- $\gamma$  production at  $\sqrt{S} = 200$  GeV may be able to distinguish between predictions based upon large and small values of  $\Delta G$ . Any sensitivity of polarized direct- $\gamma$  production to  $k_T$  smearing effects should cancel out when the asymmetries are calculated, which should eliminate some of the potential theoretical uncertainties. Furthermore, using both PHENIX and STAR to measure direct photon production will enlarge the rapidity range, and thus increase the sensitivity to extract useful physics information from this process.

We have also shown that Jet production provides an excellent mechanism to distinguish among polarized gluon models, as well as polarized quark distribution models. The corresponding predicted asymmetries are large enough to measure and distinct enough to distinguish among many models, including those mentioned in the last section and other extreme models, such as a saturated  $\Delta G$  model. [17] It is important to stress that it is necessary to include both triggering and endcap detection in STAR for the fullest coverage of  $x$ . This will help not only determine the size, but also the shape of  $\Delta G$ . The jet production rates appear to be sufficient in the appropriate kinematic regions, [18] but detection must be complete to extract the maximum physics information. The two processes discussed above seem to have greater size and more significant differences in the various predicted asymmetries than  $J/\psi$  production for the same kinematic regions. [19] It is thus important that experimental errors be minimized for both PHENIX and STAR so that these measurements can be made.

Since HERA- $\vec{N}$  coverage for direct- $\gamma$  production is at lower cms energy and spans a lower  $p_T$  range, this experiment would be complementary with that of RHIC in the gluon kinematical region covered. The sensitivity of HERA- $\vec{N}$  to  $\Delta G$  for direct- $\gamma$  production is sufficient to distinguish between the various gluon models. [20] Coupling this with the other planned experiments at HERA- $\vec{N}$  would span a sufficient kinematic range to give a very good indication as to both the size and shape of  $\Delta G$ . [21]

There are significant enough differences in the models for the gluon distributions [2,7,15,17] to warrant careful study of these processes. Measurement of asymmetries for direct photon production and jet production at RHIC and HERA- $\vec{N}$  are crucial in determining the size and shape of the polarized gluon distribution.

## ACKNOWLEDGMENTS

The work at Argonne National Laboratory was supported by the US Department of Energy, Division of High Energy Physics, Contract number W-31-109-ENG-38. LEG acknowledges the hospitality of the FNAL theory group where part of this work was completed. GPR gratefully acknowledges discussions on experimental parameters with A. Vasiliev and S. Vigdor.

## APPENDIX: X-SPACE EVOLUTION

In this appendix we give details of our  $x$ -space evolution of the polarized parton densities. We use the definitions of ref. [4] for the non-singlet distributions and splitting functions.

Starting at  $Q_0$  with  $N_f = 3$  flavours we define non-singlet distributions

$$\Delta q_i^\pm = \Delta q_i \pm \Delta \bar{q}_i \quad (\text{A1})$$

and evolve the distributions  $\Delta q_i^-$  and  $\Delta q_i^+ - \Delta q_j^+$  according to the equations

$$\frac{d(\Delta q_i^+ - \Delta q_j^+)(x, Q^2)}{d \ln Q^2} = \frac{\alpha_s(Q^2)}{2\pi} \Delta P_{qq}^+(x) * (\Delta q_i^+ - \Delta q_j^+)(x, Q^2) \quad (\text{A2})$$

and

$$\frac{d\Delta q_i^-(x, Q^2)}{d \ln Q^2} = \frac{\alpha_s(Q^2)}{2\pi} \Delta P_{qq}^-(x) * \Delta q_i^-(x, Q^2) \quad (\text{A3})$$

where

$$\Delta P_{qq}^\pm = P_{qq}^V \pm \Delta P_{q\bar{q}}^V. \quad (\text{A4})$$

The singlet distribution is defined in Eq. (3.3) and the evolution equation is given by Eq. (3.4). In ref. [4] the definition

$$\Delta P_{qq} = \Delta P_{qq}^+ + \Delta P_{qq}^S \quad (\text{A5})$$

is used. All the splitting functions are given in that reference.

For  $N_f = 3$  flavours we have four non-singlet distributions to evolve

$$\begin{aligned} T_3 &= \Delta u^+ - \Delta d^+ = \Delta u + \Delta \bar{u} - \Delta d - \Delta \bar{d} \\ T_8 &= \Delta u^+ + \Delta d^+ - 2\Delta s^+ = \Delta u + \Delta \bar{u} + \Delta d + \Delta \bar{d} - 4\Delta s \\ V_1 &= \Delta u - \Delta \bar{u} \\ V_2 &= \Delta d - \Delta \bar{d}. \end{aligned} \quad (\text{A6})$$

plus the singlet quark

$$\Sigma = \Delta u + \Delta \bar{u} + \Delta d + \Delta \bar{d} + 2\Delta s \quad (\text{A7})$$

and gluon,  $\Delta G$ , distributions. We have assumed that  $\Delta s = \Delta \bar{s}$ . The functional forms of the input distributions are given in reference [2].

We label the coefficient functions for the different sectors by  $A_n^{NS,+}$ ,  $A_n^{NS,-}$ ,  $A_n^\Sigma$  and  $A_n^G$  and correspondingly for the  $B$ 's. In LO the coefficients are given by the relations;

$$\begin{aligned} A_{n+1}^{NS,\pm}(x) &= A_n^{NS,\pm}(x) \left[ -\frac{3C_F}{\beta_0} - \frac{4C_F}{\beta_0} \ln(1-x) \right] \\ &+ \frac{2C_F}{\beta_0} \int_x^1 \frac{dy}{y} (1+z) A_n^{NS,\pm}(y) - \frac{4C_F}{\beta_0} \int_x^1 \frac{dy}{y} \frac{y A_n^{NS,\pm}(y) - x A_n^{NS,\pm}(x)}{y-x} \end{aligned} \quad (\text{A8})$$

$$\begin{aligned} A_{n+1}^\Sigma(x) &= A_n^\Sigma(x) \left[ -\frac{3C_F}{\beta_0} - \frac{4C_F}{\beta_0} \ln(1-x) \right] \\ &+ \frac{2}{\beta_0} \int_x^1 \frac{dy}{y} \left\{ C_F(1+z) A_n^\Sigma(y) - N_f(2z-1) A_n^G(y) \right\} \\ &- \frac{4C_F}{\beta_0} \int_x^1 \frac{dy}{y} \frac{y A_n^\Sigma(y) - x A_n^\Sigma(x)}{y-x} \end{aligned} \quad (\text{A9})$$

$$\begin{aligned} A_{n+1}^G(x) &= -A_n^G(x) \left[ 1 + \frac{4N_c}{\beta_0} \ln(1-x) \right] \\ &- \frac{2}{\beta_0} \int_x^1 \frac{dy}{y} \left\{ (2-z) A_n^\Sigma(y) - \frac{4N_c}{\beta_0} (2z-1) A_n^G(y) \right\} \\ &+ \int_x^1 \frac{dy}{y} \frac{y A_n^G(y) - x A_n^G(x)}{y-x} \end{aligned} \quad (\text{A10})$$

where  $z = x/y$ .

The NLO coefficients are given by;

$$\begin{aligned}
B_{n+1}^{NS,\pm}(x) = & -\frac{\beta_1}{4\pi\beta_0}A_{n+1}^{NS,\pm}(x) - B_n^{NS,\pm}(x) \left[ 1 + \frac{C_F}{\beta_0}(3 + 4\ln(1-x)) \right] + \frac{C_F}{\pi\beta_0} \left[ N_F \left( \frac{1}{12} + \frac{\pi^2}{9} \right. \right. \\
& + \left. \frac{10}{9} \ln(1-x) \right) - C_F \left( \frac{3}{8} - \frac{\pi^2}{2} + 6\zeta \right) - N_c \left( \frac{17}{24} + \frac{11\pi^2}{18} - 3\zeta + \left( \frac{67}{9} \right. \right. \\
& \left. \left. - \frac{\pi^2}{3} \right) \ln(1-x) \right) \Big] A_n^{NS,\pm}(x) + \int_x^1 \frac{dy}{y} \left[ -\frac{4C_F y B_n^{NS,\pm}(y) - x B_n^{NS,\pm}(x)}{\beta_0 (y-x)} \right. \\
& + \left. \frac{2C_F}{\beta_0}(1+z)B_n^{NS,\pm}(y) + \frac{C_F}{\beta_0\pi} \left( \frac{10}{9}N_f - N_c \left( \frac{67}{9} - \frac{\pi^2}{3} \right) \right) \right. \\
& \left. \frac{yA_n^{NS,\pm}(y) - xA_n^{NS,\pm}(x)}{y-x} - \frac{1}{\pi\beta_0} \Delta P_{qq}^{(1),\pm}(z) A_n^{NS,\pm}(y) \right], \tag{A11}
\end{aligned}$$

$$\begin{aligned}
B_{n+1}^\Sigma(x) = & -\frac{\beta_1}{4\pi\beta_0}A_{n+1}^\Sigma(x) - B_n^\Sigma(x) \left[ 1 + \frac{C_F}{\beta_0}(3 + 4\ln(1-x)) \right] + \frac{C_F}{\pi\beta_0} \left[ N_F \left( \frac{1}{12} + \frac{\pi^2}{9} \right. \right. \\
& + \left. \frac{10}{9} \ln(1-x) \right) - C_F \left( \frac{3}{8} - \frac{\pi^2}{2} + 6\zeta \right) - N_c \left( \frac{17}{24} + \frac{11\pi^2}{18} - 3\zeta + \left( \frac{67}{9} \right. \right. \\
& \left. \left. - \frac{\pi^2}{3} \right) \ln(1-x) \right) \Big] A_n^\Sigma(x) + \int_x^1 \frac{dy}{y} \left[ -\frac{4C_F y B_n^\Sigma(y) - x B_n^\Sigma(x)}{\beta_0 (y-x)} \right. \\
& + \left. \frac{2C_F}{\beta_0}(1+z)B_n^\Sigma(y) + \frac{C_F}{\beta_0\pi} \left( \frac{10}{9}N_f - N_c \left( \frac{67}{9} - \frac{\pi^2}{3} \right) \right) \frac{yA_n^\Sigma(y) - xA_n^\Sigma(x)}{y-x} \right. \\
& - \left. \frac{1}{\pi\beta_0} (\Delta P_{gg}^{(1)}(z)A_n^G(y) + \Delta P_{qq}^+(z)A_n^\Sigma(y)) \right. \\
& - \left. \frac{2N_f}{\beta_0}(2z-1)B_n^G(y) - \frac{C_F N_f}{\pi\beta_0} \{ (1-z) - (1-3z)\ln z \right. \\
& \left. - (1+z)\ln^2 z \} A_n^\Sigma(y) \right], \tag{A12}
\end{aligned}$$

$$\begin{aligned}
B_{n+1}^G(x) = & -\frac{\beta_1}{4\pi\beta_0}A_{n+1}^G(x) - B_n^G(x) \left( 2 + \frac{4N_c}{\beta_0} \ln(1-x) \right) - \frac{1}{\pi\beta_0} A_n^G(x) \left[ N_c^2 \left( \frac{8}{3} \right. \right. \\
& + \left. 3\zeta \right) - \frac{C_F N_f}{2} - \frac{2N_c N_f}{3} + \left\{ N_c^2 \left( \frac{67}{9} - \frac{\pi}{3} \right) \right. \\
& \left. - \frac{10N_f N_c}{9} \right\} \ln(1-x) \Big] + \int_x^1 \frac{dy}{y} \left[ -\frac{4N_c y B_n^G(y) - x B_n^G(x)}{\beta_0 (y-x)} \right. \\
& - \left. \frac{2C_F}{\beta_0}(2-z)B_n^\Sigma(y) + \frac{4N_c}{\beta_0}(2z-1)B_n^G(y) - \frac{1}{\pi\beta_0} \left( N_c^2 \left( \frac{67}{9} - \frac{\pi^2}{3} \right) \right. \right. \\
& \left. \left. - \frac{10N_c}{9} \right) \frac{yA_n^G(y) - xA_n^G(x)}{y-x} - \frac{1}{\pi\beta_0} (\Delta P_{gg}^{(1)}(z)A_n^\Sigma(y) + \Delta P_{qq}^{(1)}(z)A_n^G(y)) \right], \tag{A13}
\end{aligned}$$

where

$$\begin{aligned}
P_{qq}^+(z) &= C_F^2 \left\{ - \left( 2 \ln(z) \ln(1-z) + \frac{3}{2} \ln(z) \right) \delta P_{qq}(z) - \left( \frac{3}{2} + \frac{7}{2}z \right) \ln(z) - \frac{1}{2}(1+z) \ln^2(z) \right. \\
&\quad \left. - 5(1-z) \right\} \\
&+ C_F N_c \left\{ \left( \frac{1}{2} \ln^2(z) + \frac{11}{6} \ln(z) \right) \delta P_{qq}(z) - \left( \frac{67}{18} - \frac{\pi^2}{6} \right) (1+z) + (1+z) \ln(z) \right. \\
&\quad \left. + \frac{20}{3}(1-z) \right\} + \frac{C_F N_f}{2} \left\{ -\frac{2}{3} \ln(z) \delta P_{qq}(z) + \frac{10}{9}(1+z) - \frac{4}{3}(1-z) \right\} \\
&- C_F \left( C_F - \frac{N_c}{2} \right) \{ 2\delta P_{qq}(-z) S_2(z) + 2(1+z) \ln(z) + 4(1-z) \}, \tag{A14}
\end{aligned}$$

$$\begin{aligned}
P_{qq}^-(z) &= C_F^2 \left\{ - \left( 2 \ln(z) \ln(1-z) + \frac{3}{2} \ln(z) \right) \delta P_{qq}(z) - \left( \frac{3}{2} + \frac{7}{2}z \right) \ln(z) - \frac{1}{2}(1+z) \ln^2(z) \right. \\
&\quad \left. - 5(1-z) \right\} \\
&+ C_F N_c \left\{ \left( \frac{1}{2} \ln^2(z) + \frac{11}{6} \ln(z) \right) \delta P_{qq}(z) - \left( \frac{67}{18} - \frac{\pi^2}{6} \right) (1+z) + (1+z) \ln(z) \right. \\
&\quad \left. + \frac{20}{3}(1-z) \right\} + \frac{C_F N_f}{2} \left\{ \frac{2}{3} \ln(z) \delta P_{qq}(z) + \frac{10}{9}(1+z) - \frac{4}{3}(1-z) \right\} \\
&+ C_F \left\{ C_F - \frac{N_c}{2} \right\} \{ 2\delta P_{qq}(-z) S_2(z) + 2(1+z) \ln(z) + 4(1-z) \}, \tag{A15}
\end{aligned}$$

$$\delta P_{qq}(z) = \frac{2}{1-z} - 1 - z, \tag{A16}$$

$$\delta P_{gg}(z) = \frac{1}{1-z} - 2z + 1, \tag{A17}$$

$$S_2 = -2\text{Li}_2(-z) - 2 \ln(z) \ln(1+z) + \frac{1}{2} \ln(z)^2 - \frac{\pi^2}{6} \tag{A18}$$

with

$$\text{Li}_2(-z) \equiv - \int_0^{-z} \frac{dx}{x} \ln(1-x) = \sum_{n=1}^{\infty} \frac{(-z)^n}{n^2}, \tag{A19}$$

$$\begin{aligned}
P_{gg}^{(1)}(z) &= \frac{C_F N_f}{2} \left\{ -\frac{4}{9}(z+4) - \frac{4}{3}(2-z) \ln(1-z) \right\} + C_F^2 \left\{ -\frac{1}{2} - \frac{1}{2}(4-z) \ln(z) \right. \\
&\quad \left. - (2+z) \ln(1-z) + \left( -4 - \ln^2(1-z) + \frac{1}{2} \ln^2(z) \right) (2-z) \right\} \\
&+ C_F N_c \left\{ (4-13z) \ln(z) + (10+z) \frac{\ln(1-z)}{3} + \frac{(41+35z)}{9} + \frac{1}{2} (-2S_2(z)) \right. \\
&\quad \left. + 3 \ln^2(z) \right\} \times (2+z) + \left( \ln^2(1-z) - 2 \ln(1-z) \ln(z) - \frac{\pi^2}{6} \right) (2-z) \Big\}, \tag{A20}
\end{aligned}$$

$$P_{gg}^{(1)}(z) = \frac{C_F N_f}{2} \{ -22 + 27z - 9 \ln(z) + 8(1-z) \ln(1-z) + (2z-1) \}$$

$$\begin{aligned}
& \left. (2 \ln^2(1-z) - 4 \ln(1-z) \ln(z) + \ln^2(z) - \frac{2\pi^2}{3}) \right\} \\
& + \frac{N_c N_f}{2} \left\{ 2(12 - 11z) - 8(1-z) \ln(1-z) + 2(1+8z) \ln(z) - 2 \left( \ln^2(1-z) - \frac{\pi^2}{6} \right) \right. \\
& \left. \times (2z-1) - (2S_2(z) - 3 \ln^2(z))(-2z-1) \right\}, \tag{A21}
\end{aligned}$$

and

$$\begin{aligned}
P'_{gg}(1)(z) &= -\frac{N_c N_f}{2} \left\{ 4(1-z) + \frac{4}{3}(1+z) \ln(z) + \frac{20}{9}(1-2z) \right\} \\
& - \frac{C_F N_f}{2} \left\{ 10(1-z) + 2(5-z) \ln(z) + 2(1+z) \ln^2(z) \right\} \\
& + N_c^2 \left\{ (29 - 67z) \frac{\ln(z)}{3} - \frac{19}{2}(1-z) + 4(1+z) \ln^2(z) - 2S_2(z) \delta P_{gg}(-z) \right. \\
& \left. + (\ln^2(z) - 4 \ln(1-z) \ln(z)) \delta P_{gg}(z) + \left( \frac{67}{9} - \frac{\pi^2}{3} \right) (1-2z) \right\}. \tag{A22}
\end{aligned}$$

## REFERENCES

- [1] M. Goshtasbpour and G. P. Ramsey, Phys. Rev. **D55**, 1244 (1997).
- [2] L. E. Gordon, M. Goshtasbpour and G. P. Ramsey, Phys. Rev. **D58**, 094017 (1998), (hep-ph/9803351).
- [3] CTEQ Collaboration, H. L. Lai *et al.*, Phys. Rev. **D51**, 4763 (1995).
- [4] R. Mertig and W. L. van Neerven, Z. Phys. **C70**, 637 (1996); W. Vogelsang, Phys. Rev. **D54**, 2023 (1996) and Nucl. Phys. **B475**, 47 (1996).
- [5] G. Rossi, Phys. Rev. **D29**, 852 (1984).
- [6] Proceedings from the RIKEN BNL Research Center Workshop, BNL, April 27-29, 1998, G. Bunce, *et. al.*, Editors; BNL-65615, vol. 7. See also Web site- <http://www.rhic.bnl.gov> for more information.
- [7] R. D. Ball, S. Forte and G. Rudolfi, Nucl. Phys. **B496**, 337 (1997); see also Altarelli, *et. al.*, hep-ph/9707276 and Acta Phys. Polon. **B29**, 1145 (1998), (hep-ph/9803237); and R. L. Jaffe, Phys. Lett. **B365**, 359 (1996).
- [8] W.-D. Nowak "Possible Measurements of Single and Double Spin Asymmetries with HERA- $\vec{N}$ ", hep-ph/9605411, published in the proceedings of the Trieste Collider Spin Physics Workshop, 169 (1995). Also see Nucl. Phys. **A622**, 78c (1997).
- [9] E. L. Berger and J. Qiu, Phys. Rev. **D40**, 778 (1989).
- [10] A. P. Contogouris, B. Kamal, Z. Merebashvili and F. V. Tkachov, Phys. Lett. **B304**, 329 (1993); Phys. Rev. **D48**, 4092 (1993).
- [11] L. E. Gordon and W. Vogelsang, Phys. Rev. **D48**, 3136 (1993) and **D49**, 170 (1994).
- [12] L. E. Gordon, Nucl. Phys. **B501**, 175 (1997) and *ibid.*, p. 197.
- [13] L. E. Gordon, Phys. Lett. **B406**, 184 (1997).
- [14] D. de Florian, S. Frixione, A. Signer and W. Vogelsang, hep-ph/9808262.
- [15] T. Gehrmann and W. J. Stirling, Phys. Rev. **D53**, 6100 (1996).
- [16] Y. Goto, see article in ref [6];  
transparencies available at URL <http://www.phenix.bnl.gov/WWW/publish/goto/>.
- [17] J. M. Virey and J. Soffer, Nucl. Phys. **B509**, 297 (1998) and C. Bourrely and J. Soffer, Nucl. Phys. **B445**, 341 (1995).
- [18] G. P. Skoro and M. V. Tokarev, Nuovo Cim. **111A**, 353 (1998).
- [19] O. Teryaev and A. Tkabladze, Phys. Rev. **D56**, 7331 (1997).
- [20] L. E. Gordon and W. Vogelsang, Phys. Lett. **B387**, 629 (1996).
- [21] A. De Roeck, A. Deshpande, V. W. Hughes, J. Lichtenstadt, and G. Radcliff, hep-ph/9801300, DESY 97-249, to appear in Eur. Phys. J. **C**.

## Figure Captions

- [1] (a) Polarized gluon distribution  $x\Delta G(x, Q^2)$  at  $Q^2 = 100 \text{ GeV}^2$  showing the GSA, GGRA, GGRB and GGRC parametrizations. (b) same as (a) for the  $\Delta\bar{u}$ -quark distribution. (c) Same as (a) and (b) for the strange quark distribution. The dotted curve near the solid (GGRA) is for the LO version of GGRA. Same as (c) for the valence u-quark distribution. Again the dotted curve near the solid curve is the LO version of GGRA. The valence distributions for GGRA, GGRB and GGRC cannot be distinguished.
- [2] (a)  $p_T$ -distribution for unpolarized prompt photon production at  $y^\gamma = 0$  for  $\sqrt{S} = 200 \text{ GeV}$ . (b) Asymmetry  $A_{LL}^\gamma$  for the cross section in (a) as predicted by the GSA, GGRA, GGRB and GGRC polarized parton distributions. (c) Asymmetries from (b) for GSA, GGRA and GGRC showing the contributions from the  $qg$  and  $q\bar{q}$  initial state contributions.
- [3] (a) Rapidity distribution for unpolarized prompt photon production at  $p_T^\gamma = 15 \text{ GeV}$  and  $\sqrt{S} = 200 \text{ GeV}$ . (b) Asymmetries for the rapidity distribution as predicted by various polarized parton parametrizations.
- [4] (a)  $p_T$ -distribution for unpolarized prompt photon production at  $y^\gamma = 0$  for  $\sqrt{S} = 40 \text{ GeV}$ . (b) Asymmetry  $A_{LL}^\gamma$  for the cross section in (a) as predicted by the GSA, GGRA, GGRB and GGRC polarized parton distributions.
- [5] (a)  $p_T$ -distribution for the unpolarized jet cross section at  $y^J = 0$  for  $\sqrt{S} = 200 \text{ GeV}$ . (b) Asymmetry  $A_{LL}^J$  for the total and for various initial state contributions as predicted by the GSA distributions. (c), (d) and (e): Same as (b) for the GGRA, GGRB and GGRC parametrizations respectively.
- [6] (a)  $p_T$ -distribution for the unpolarized jet cross section at  $y^J = 0$  for  $\sqrt{S} = 500 \text{ GeV}$ . (b) Asymmetry  $A_{LL}^J$  for the cross section as predicted by the GSA, GGRA, GGRB and GGRC polarized distributions.



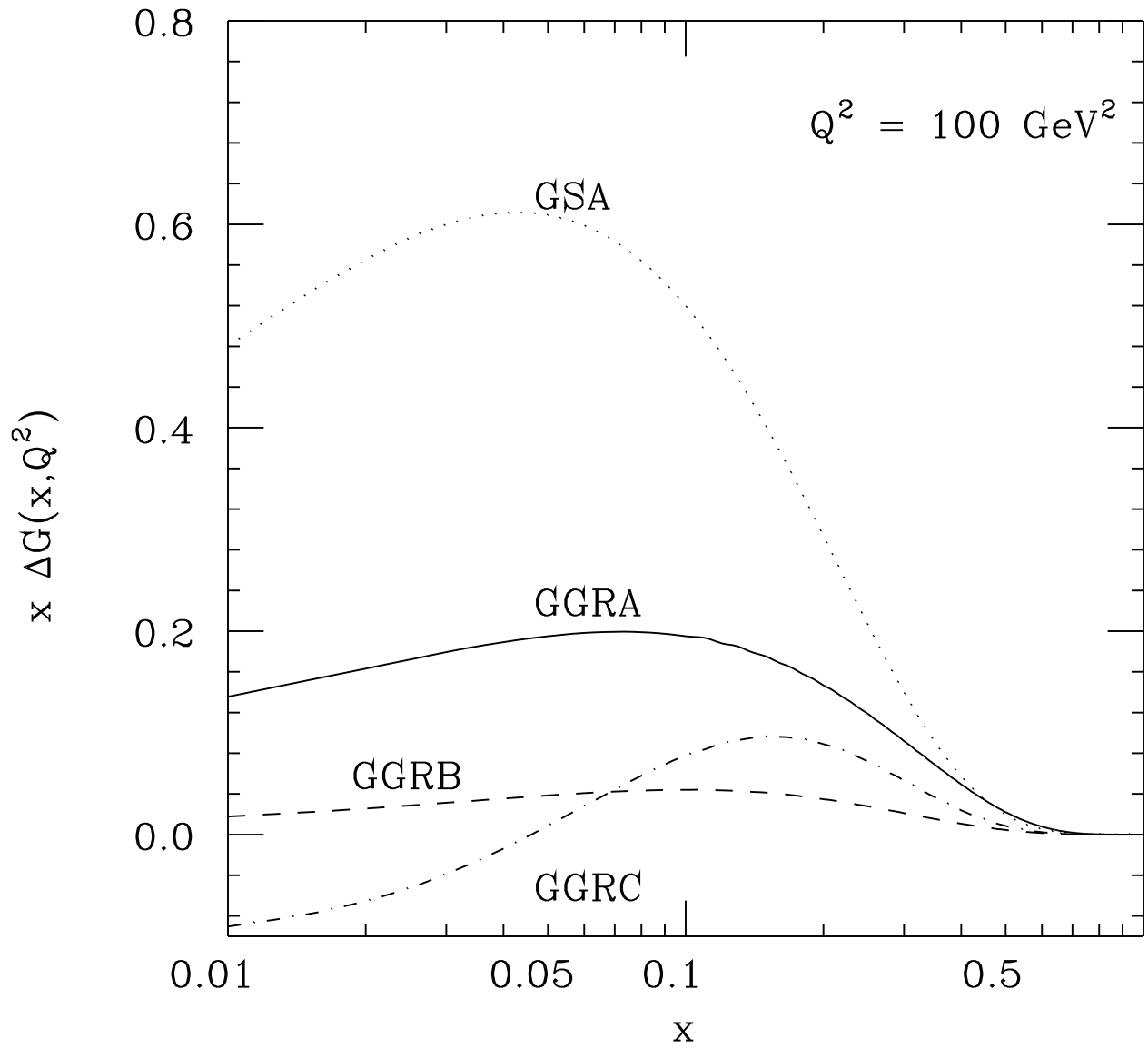


Fig. 1a

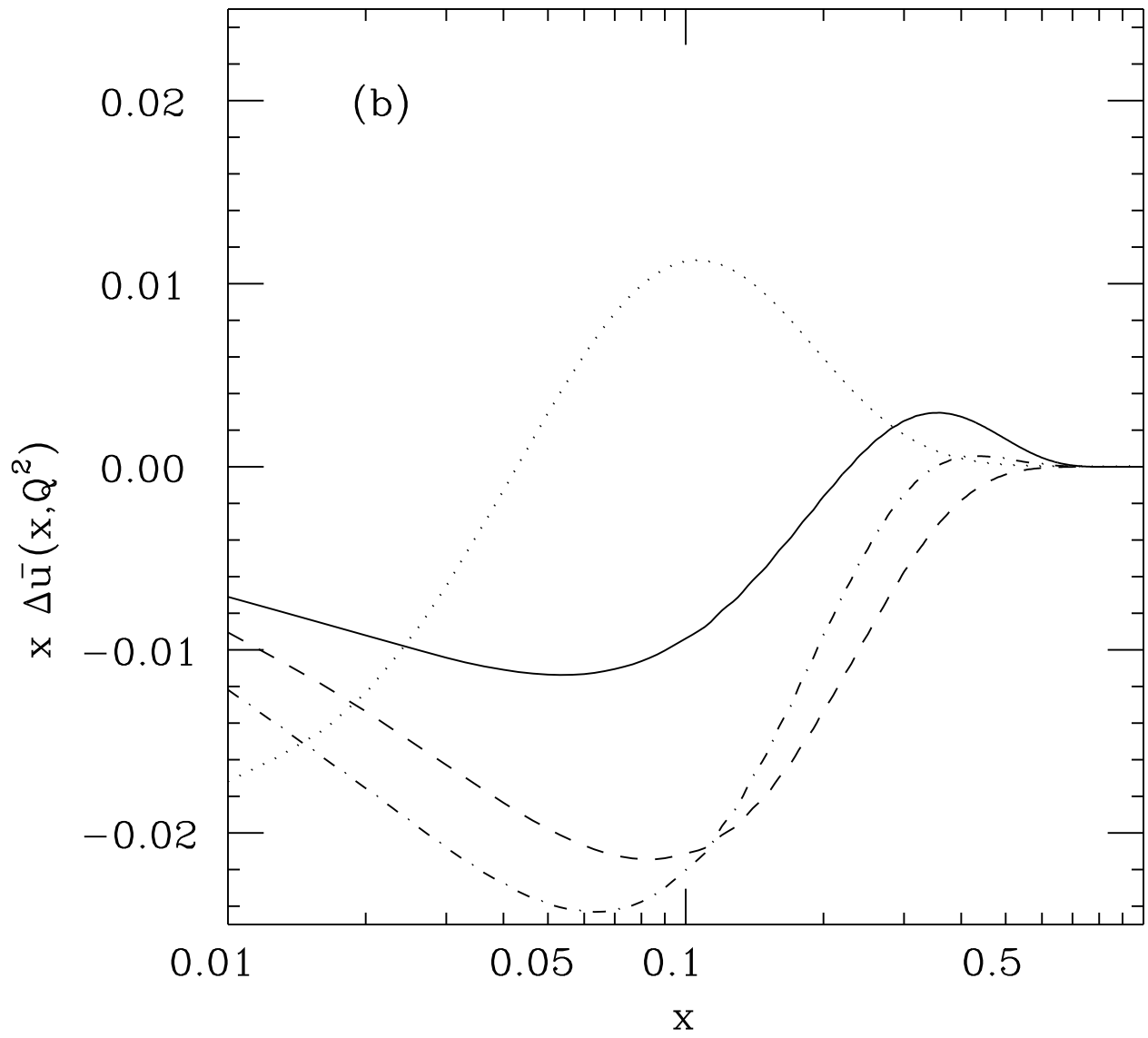


Fig. 1b

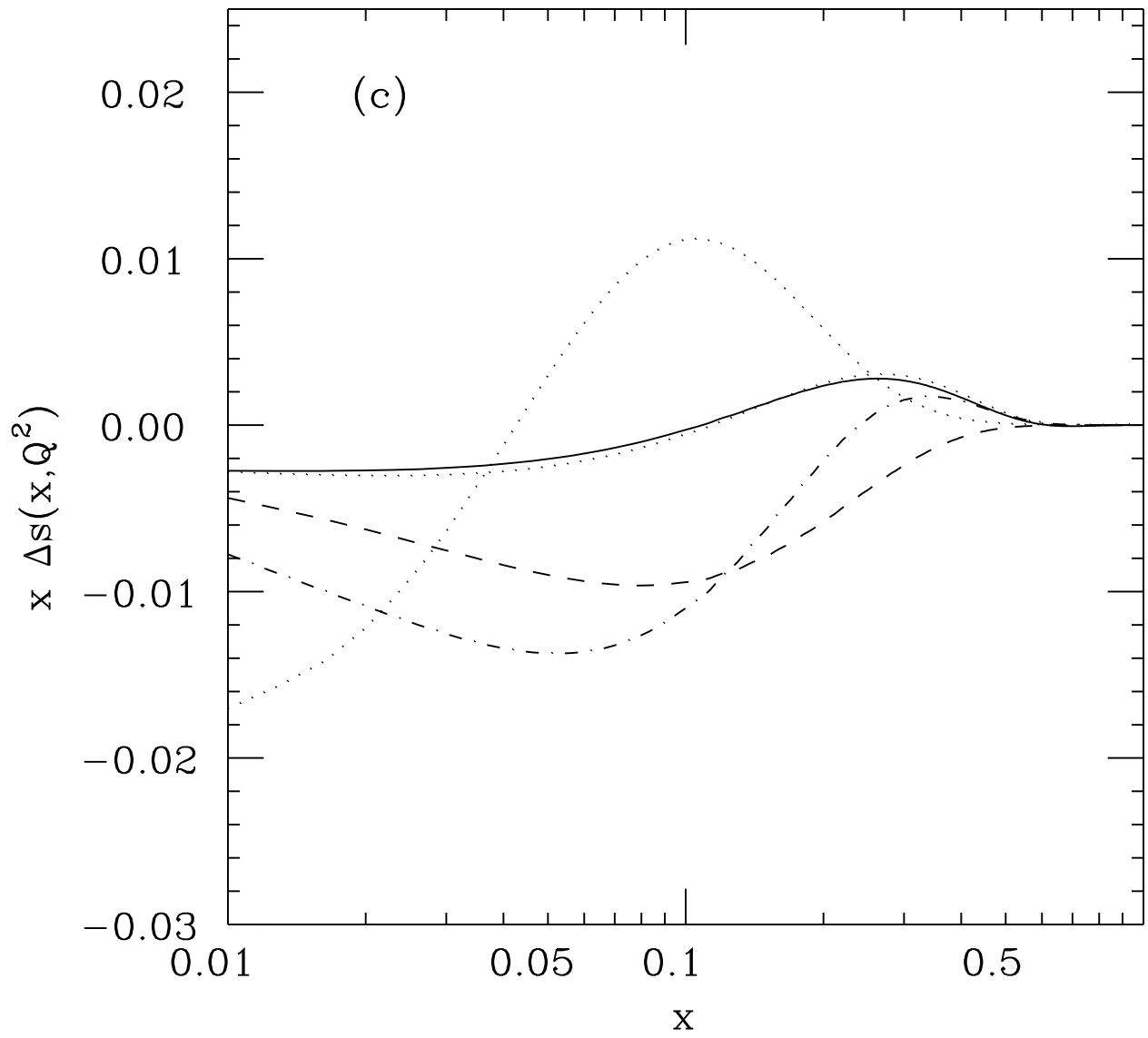


Fig. 1c

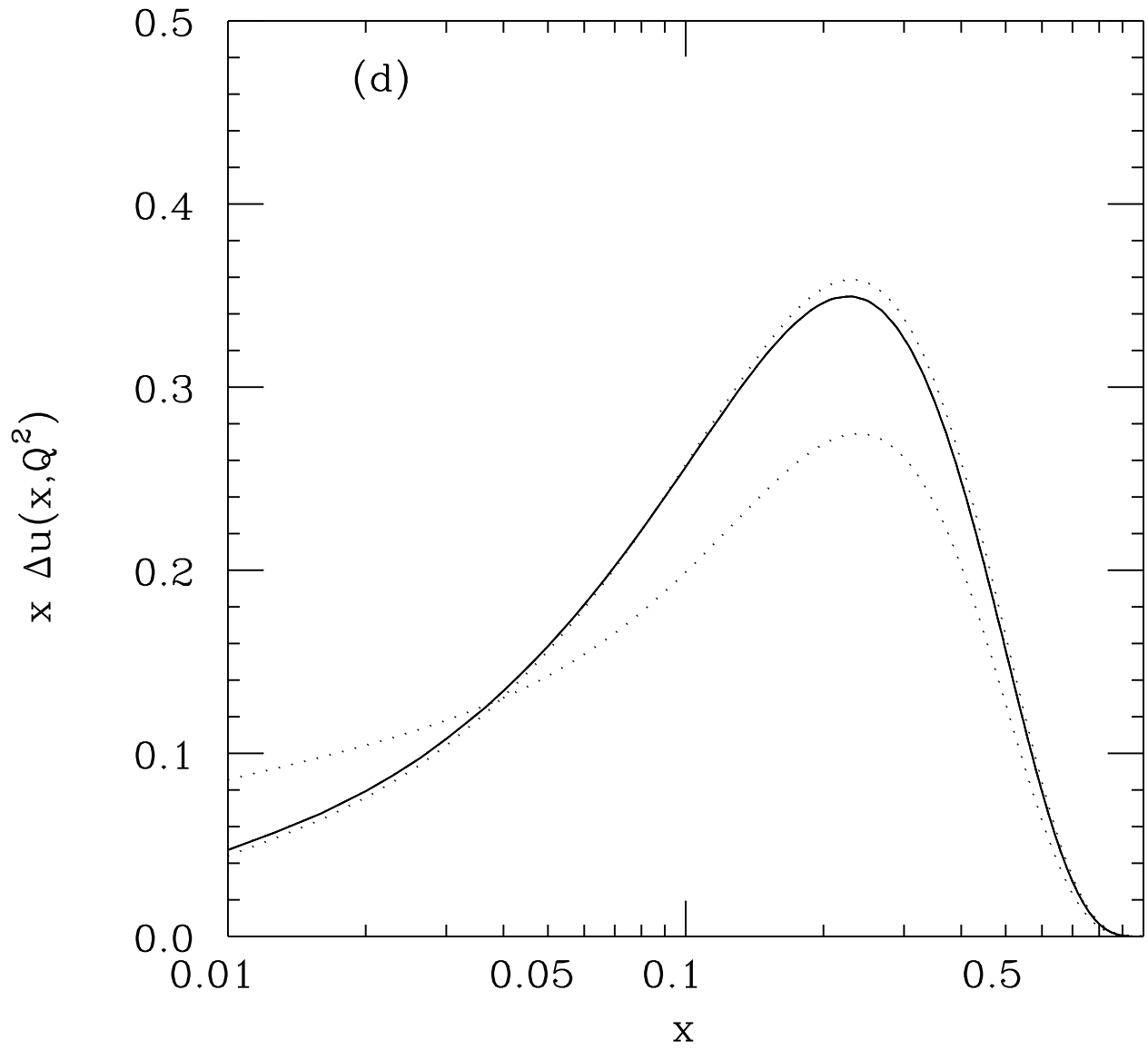


Fig. 1d

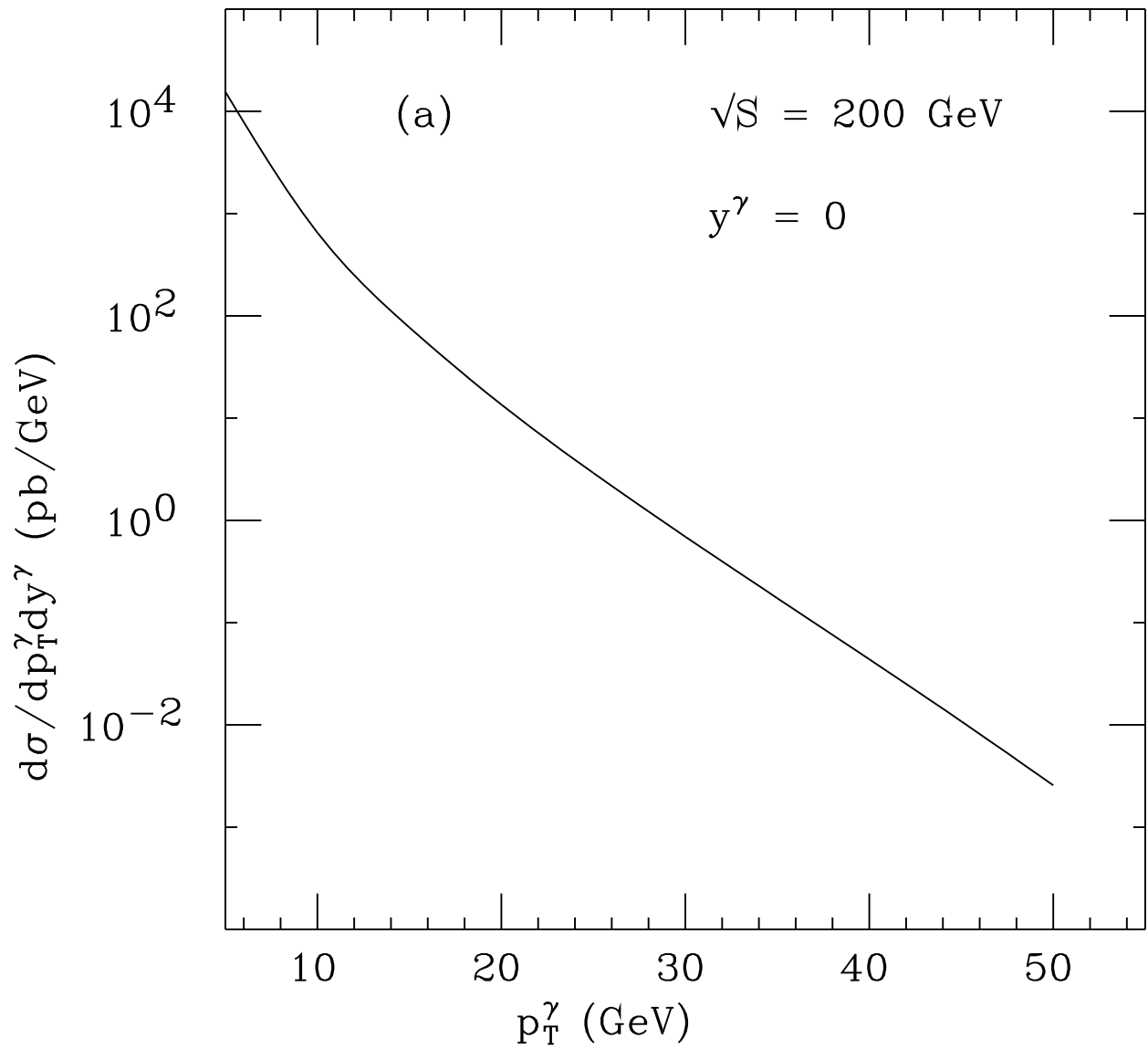


Fig. 2a

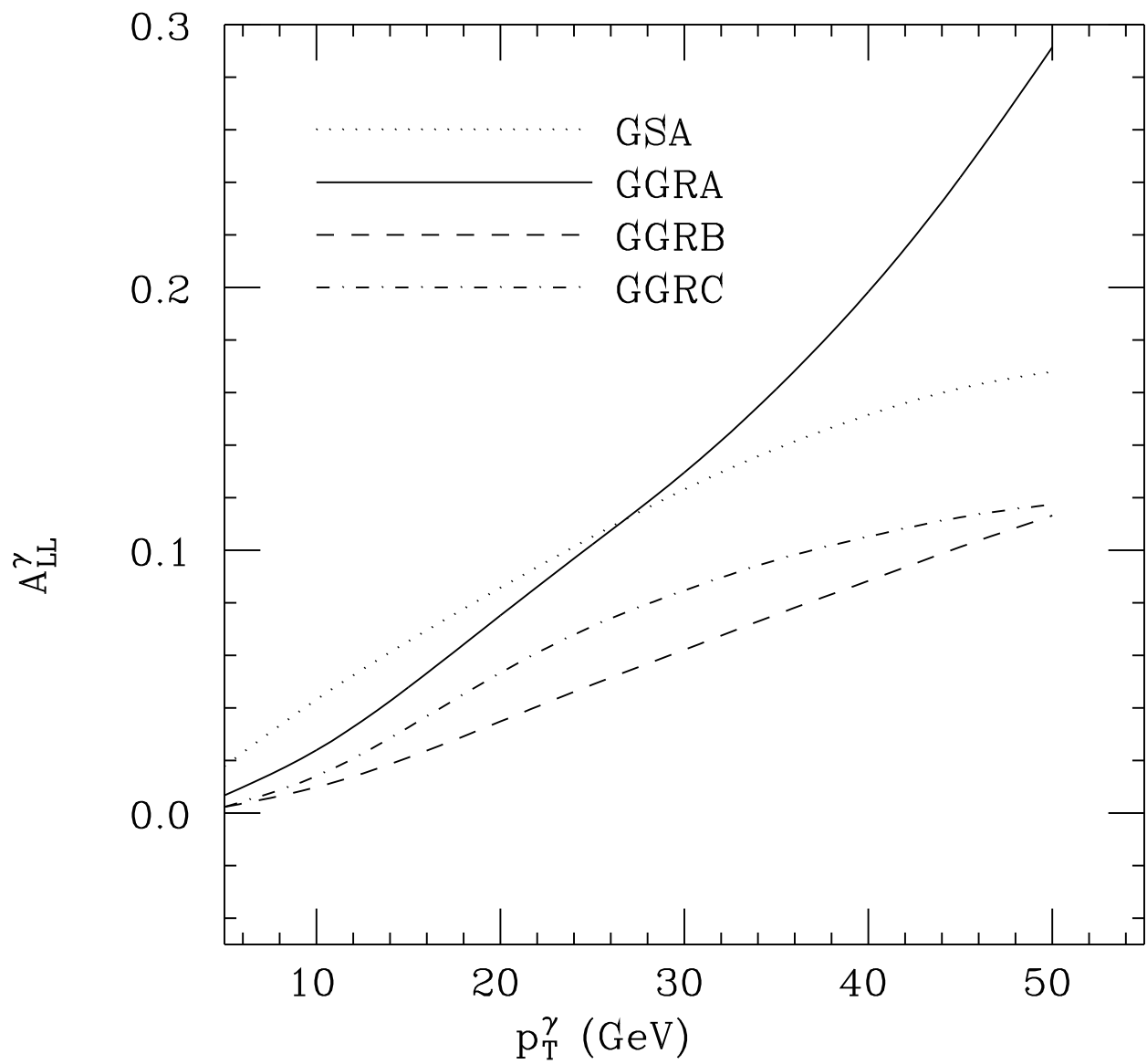


Fig. 2b

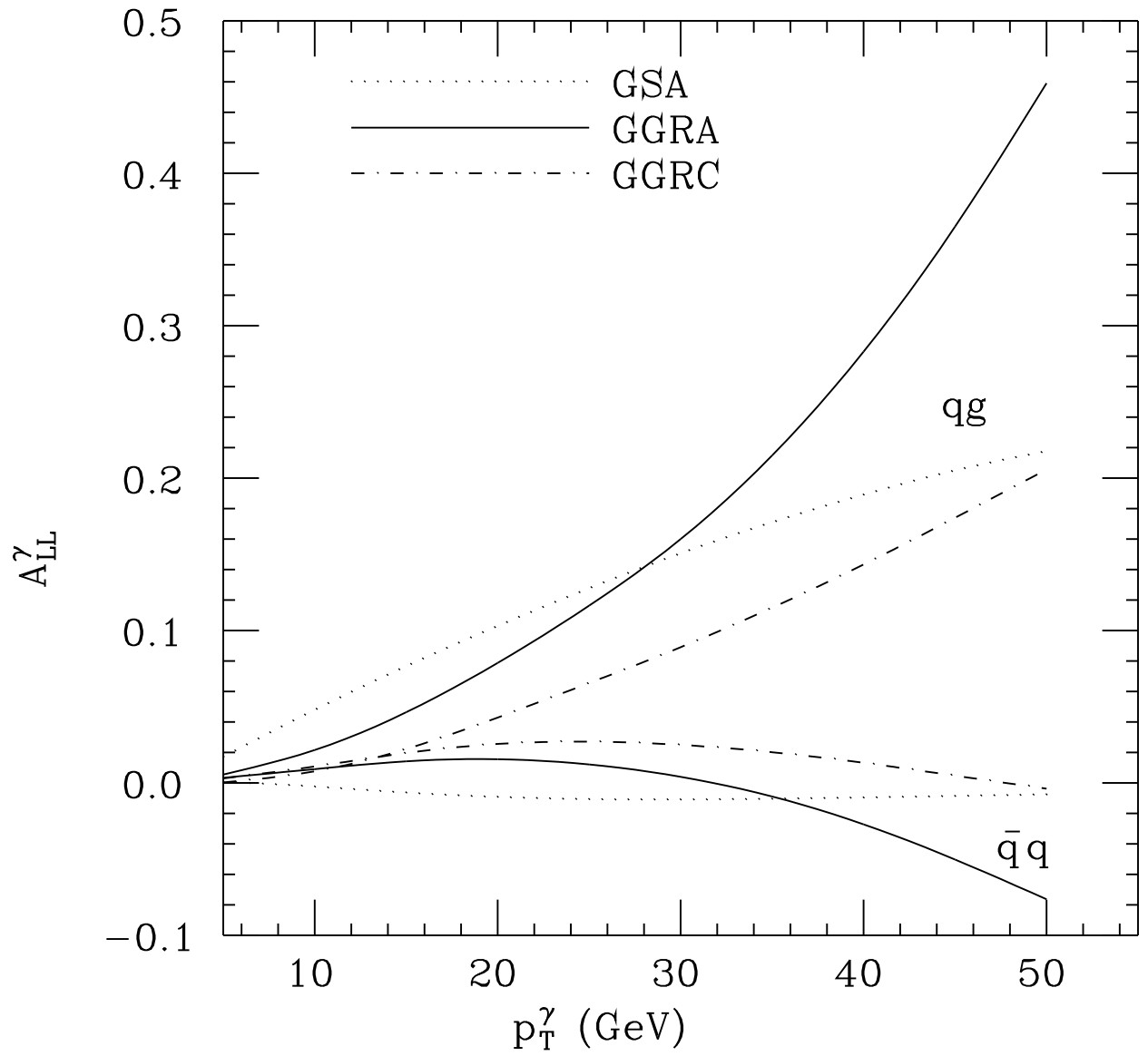


Fig. 2c

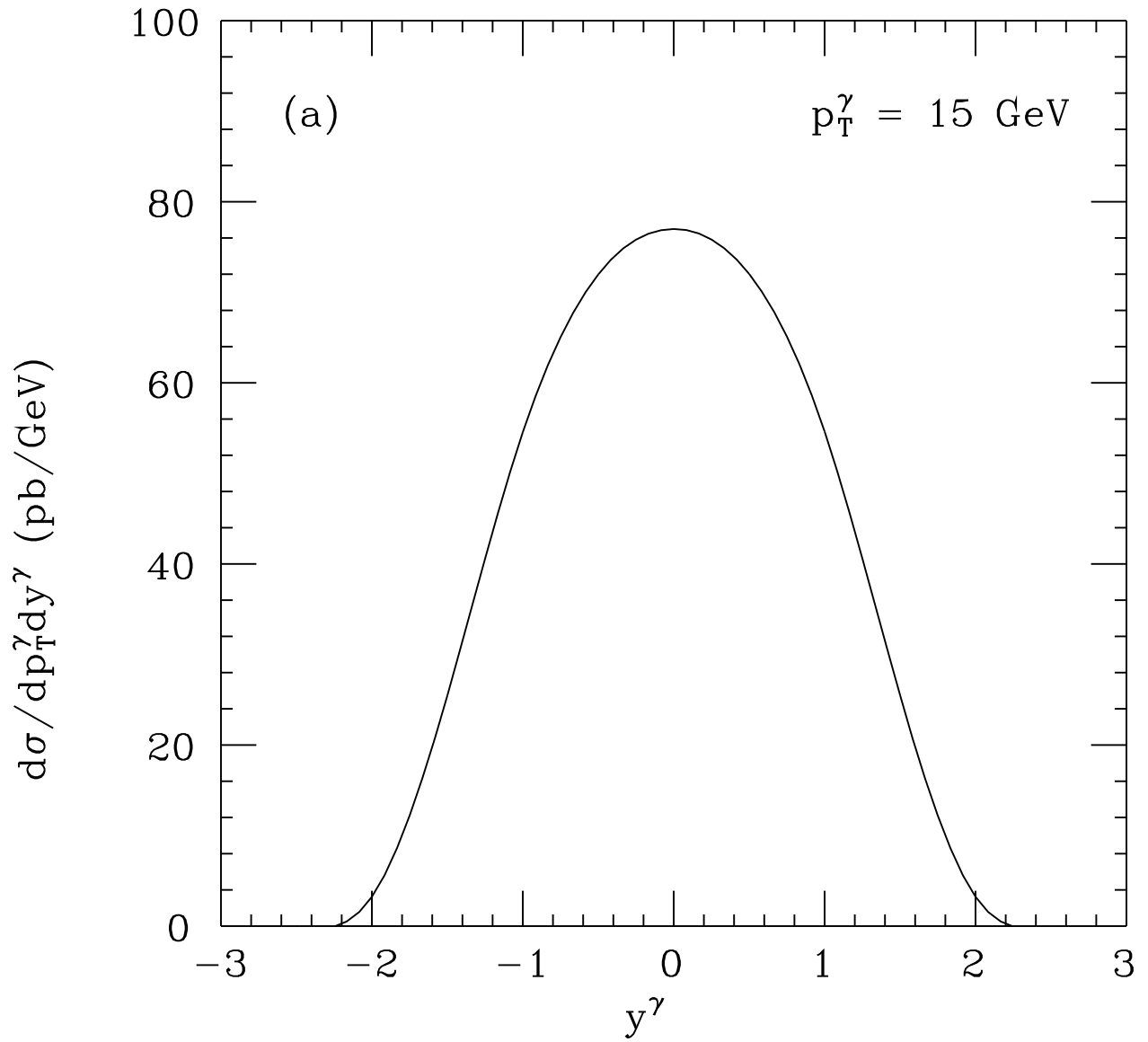


Fig. 3a



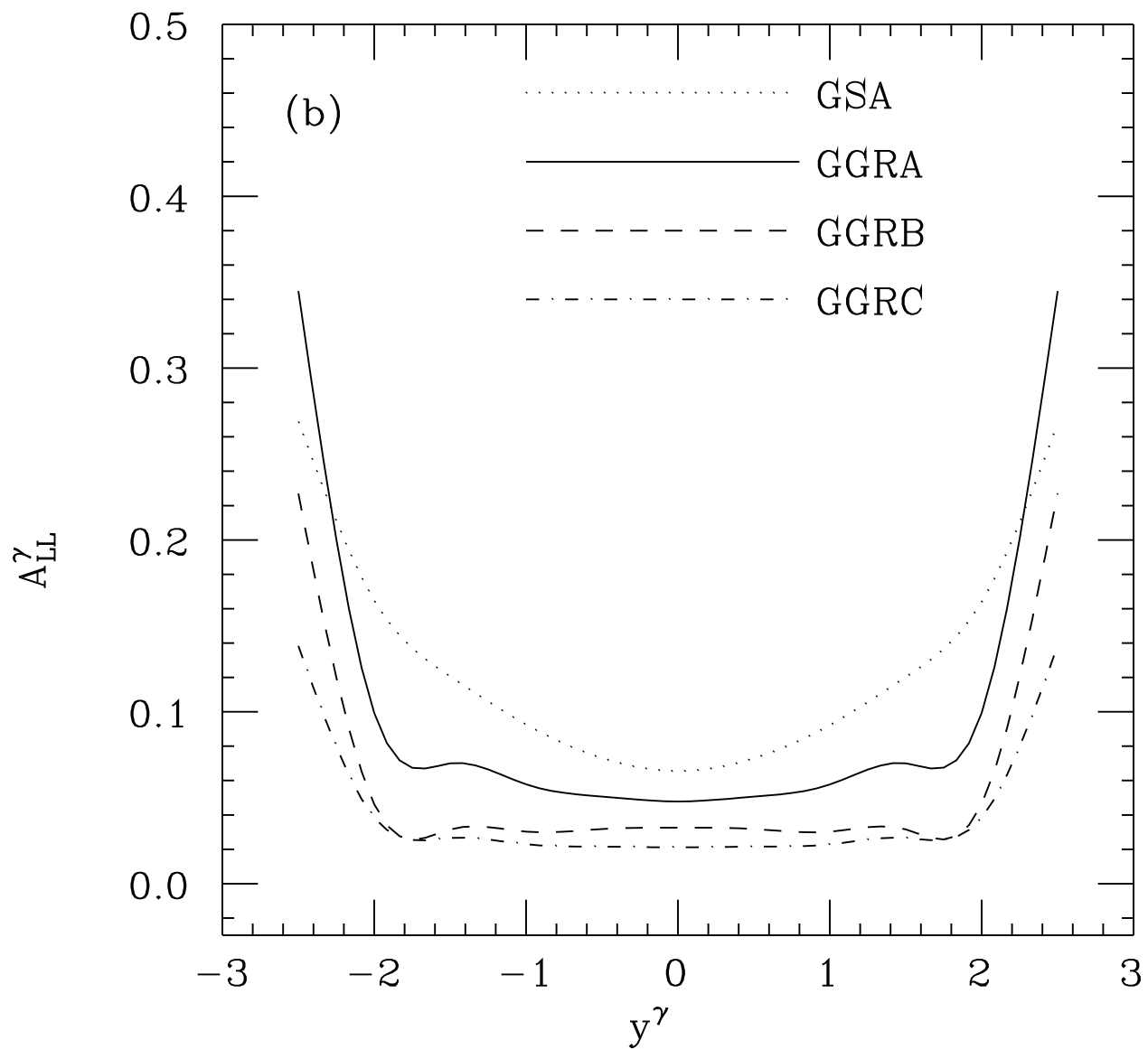


Fig. 3b

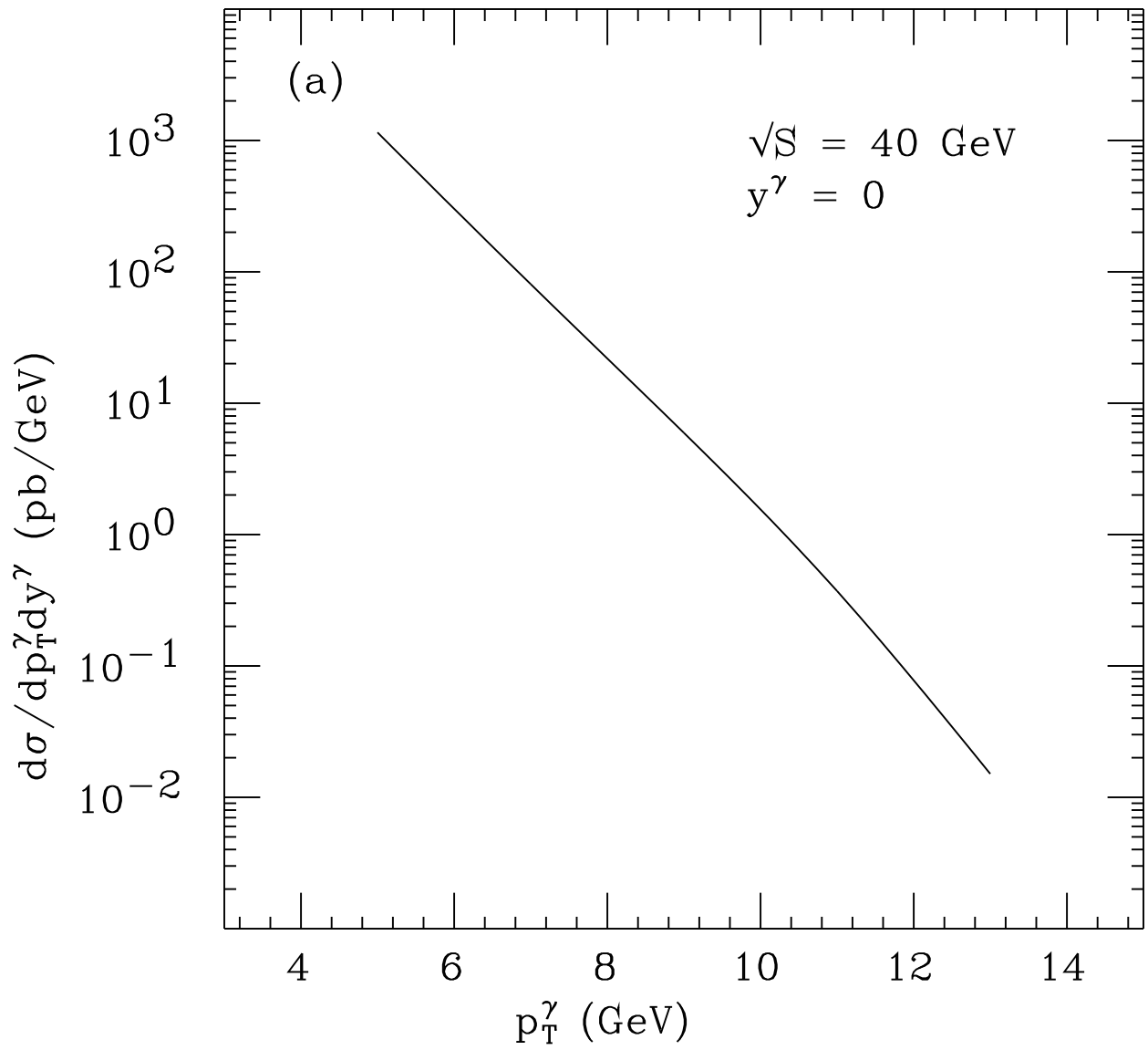


Fig. 4a

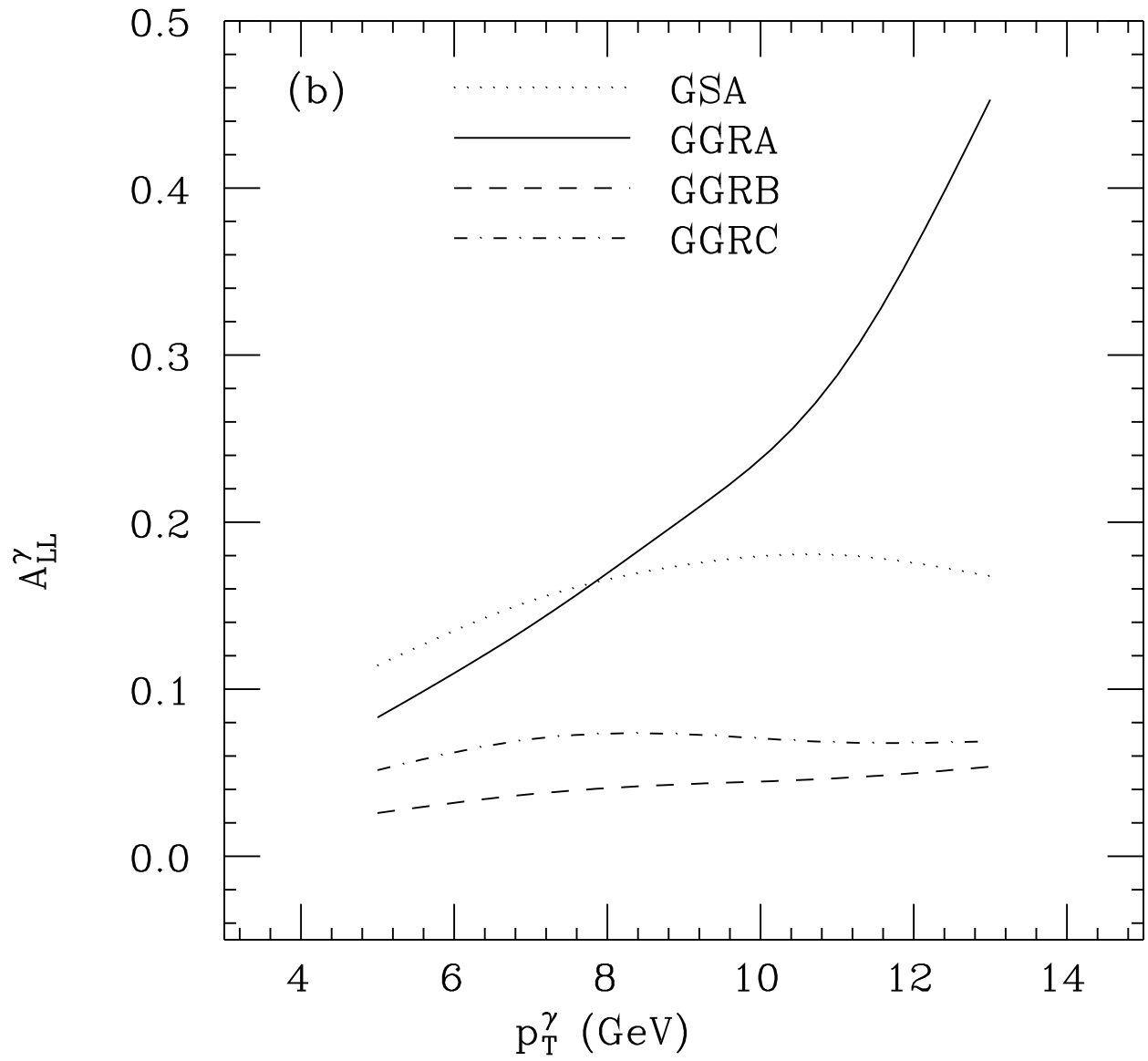


Fig. 4b

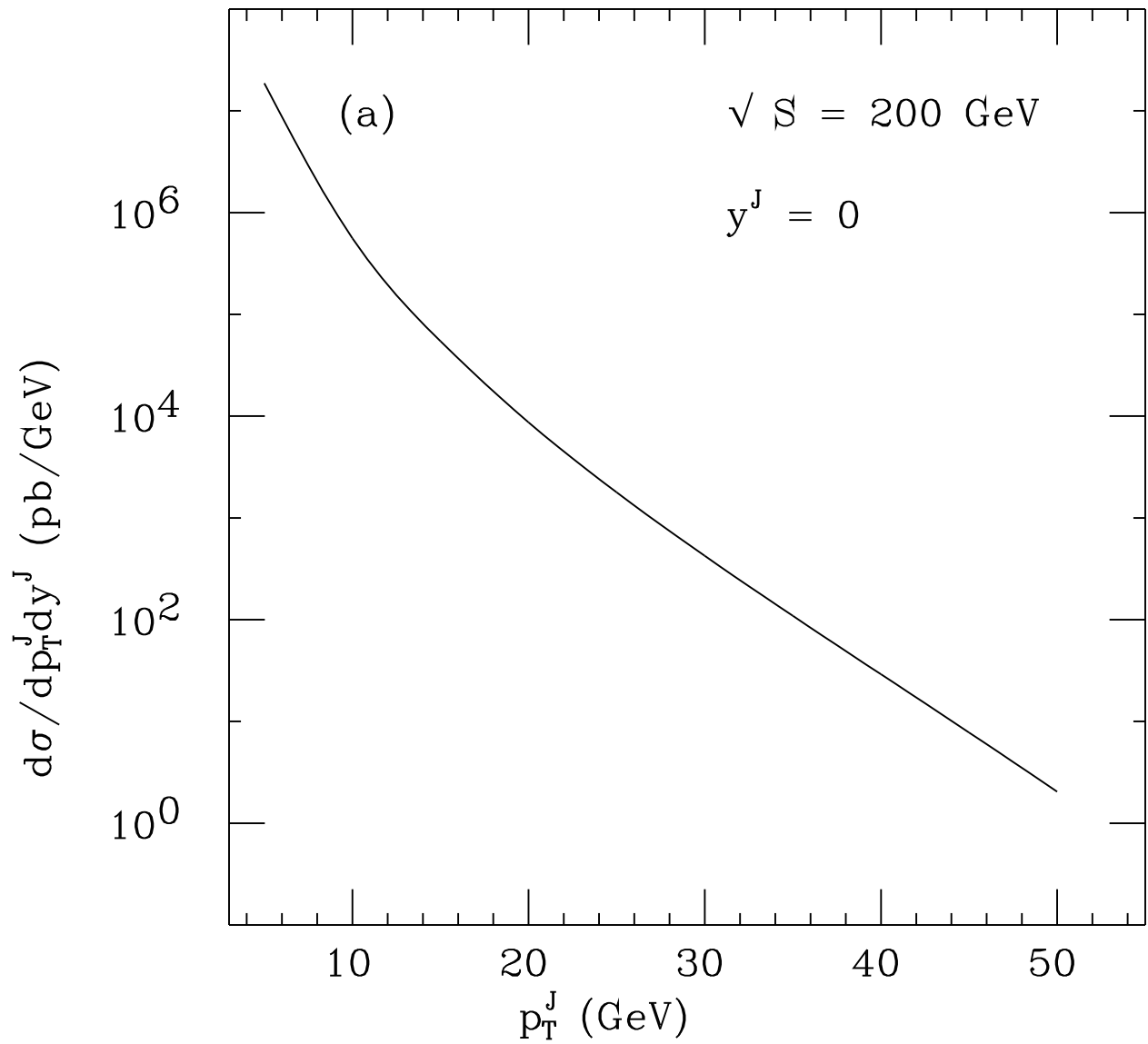


Fig. 5a

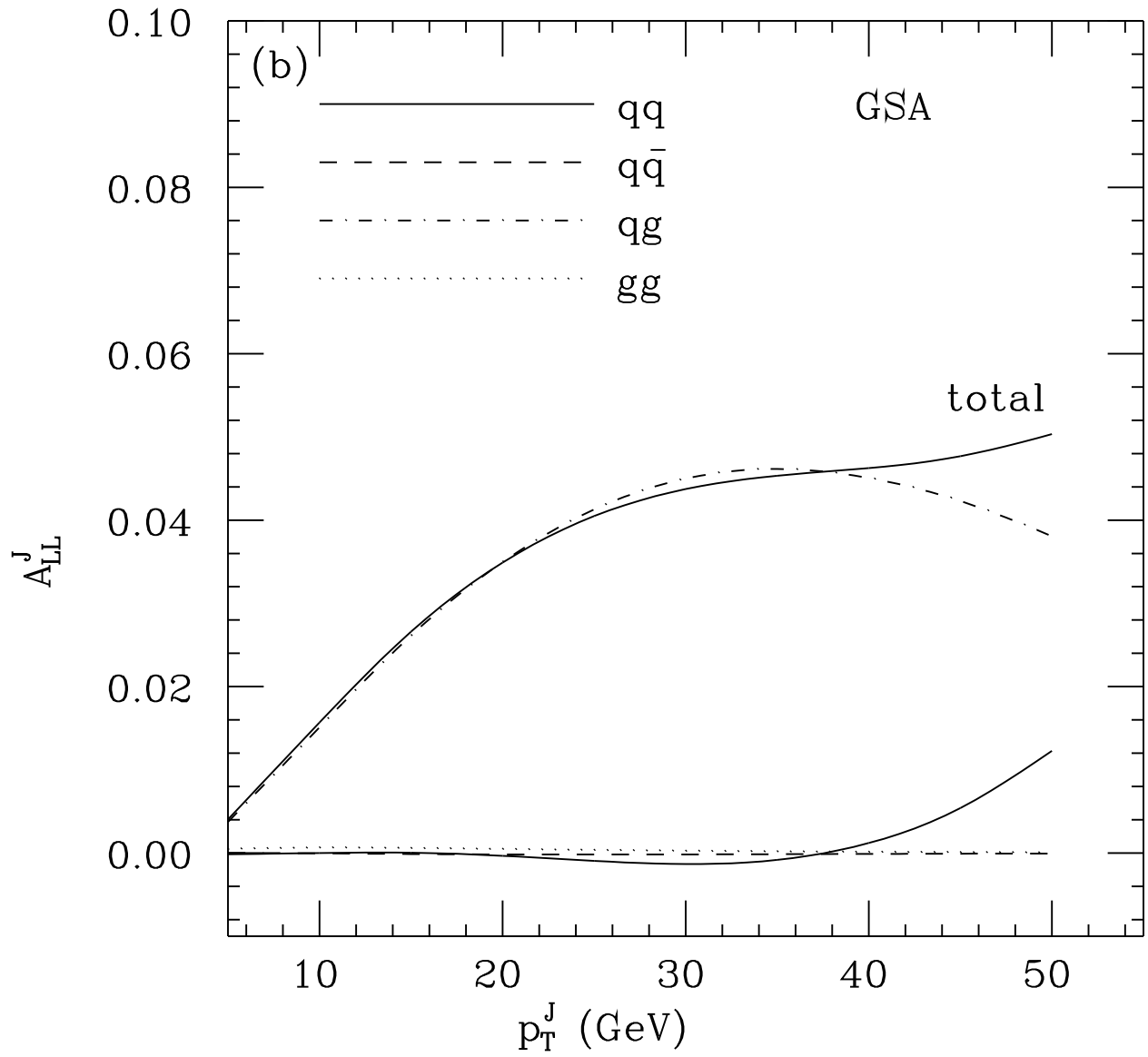


Fig. 5b

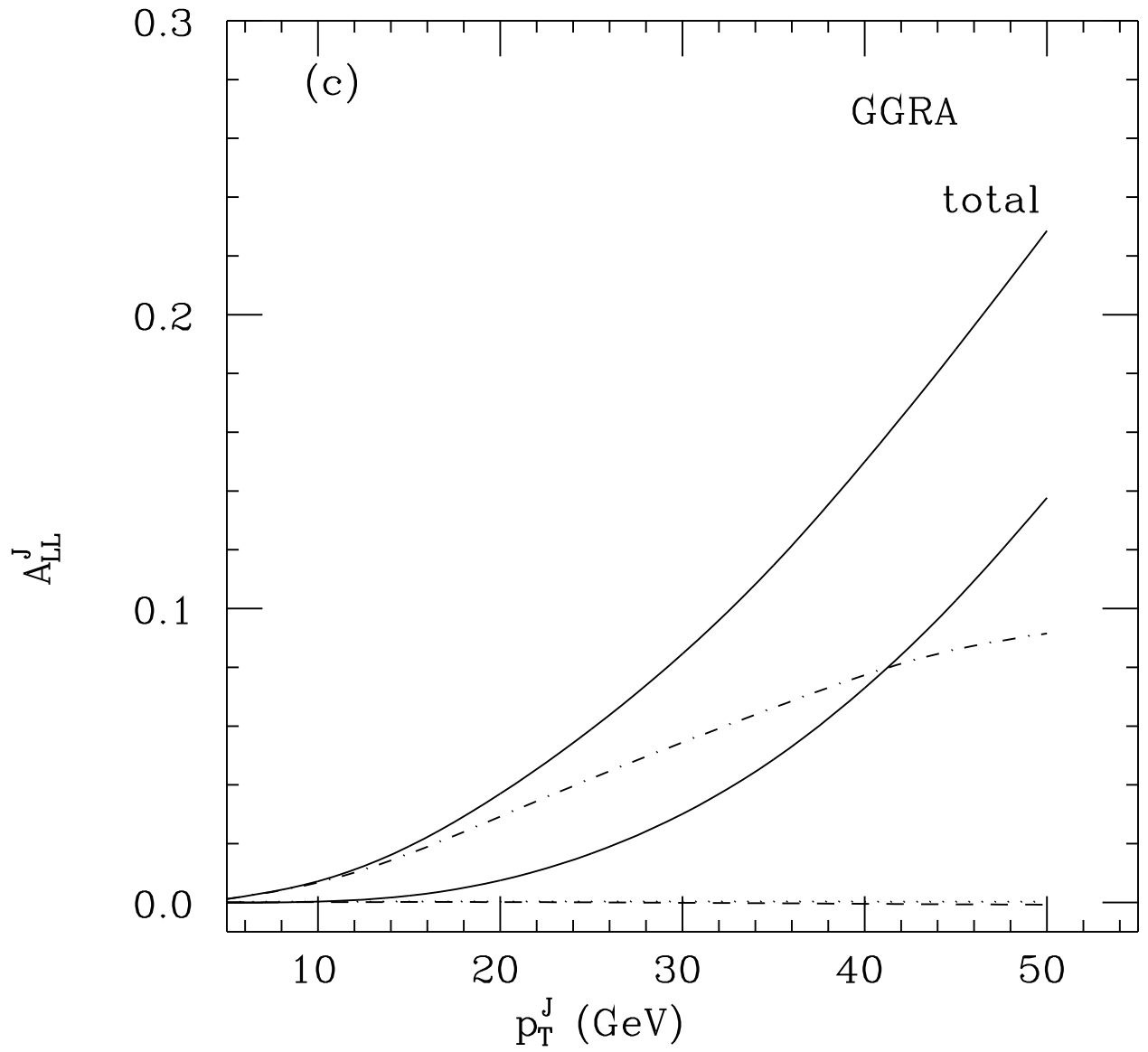


Fig. 5c

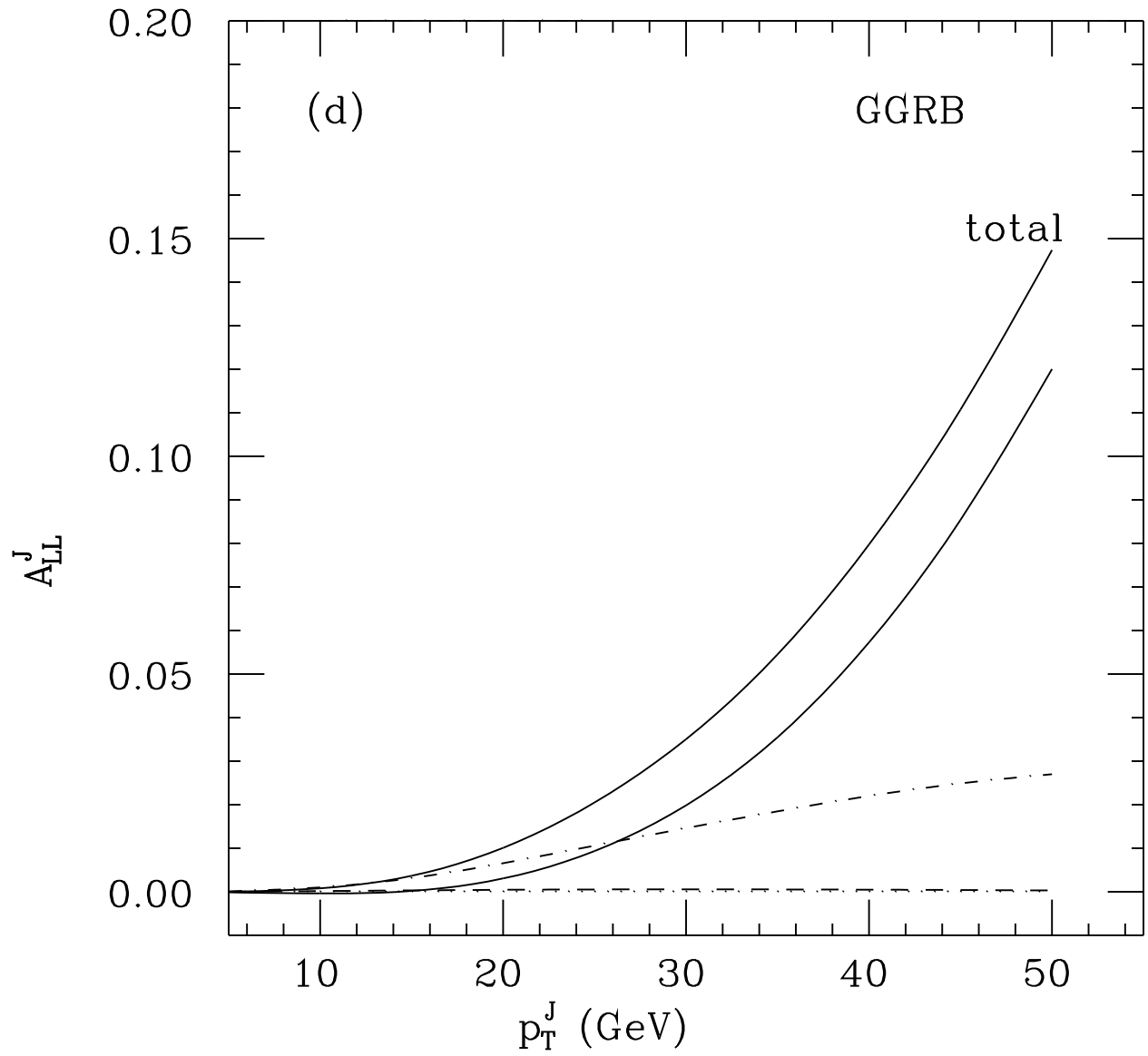


Fig. 5d

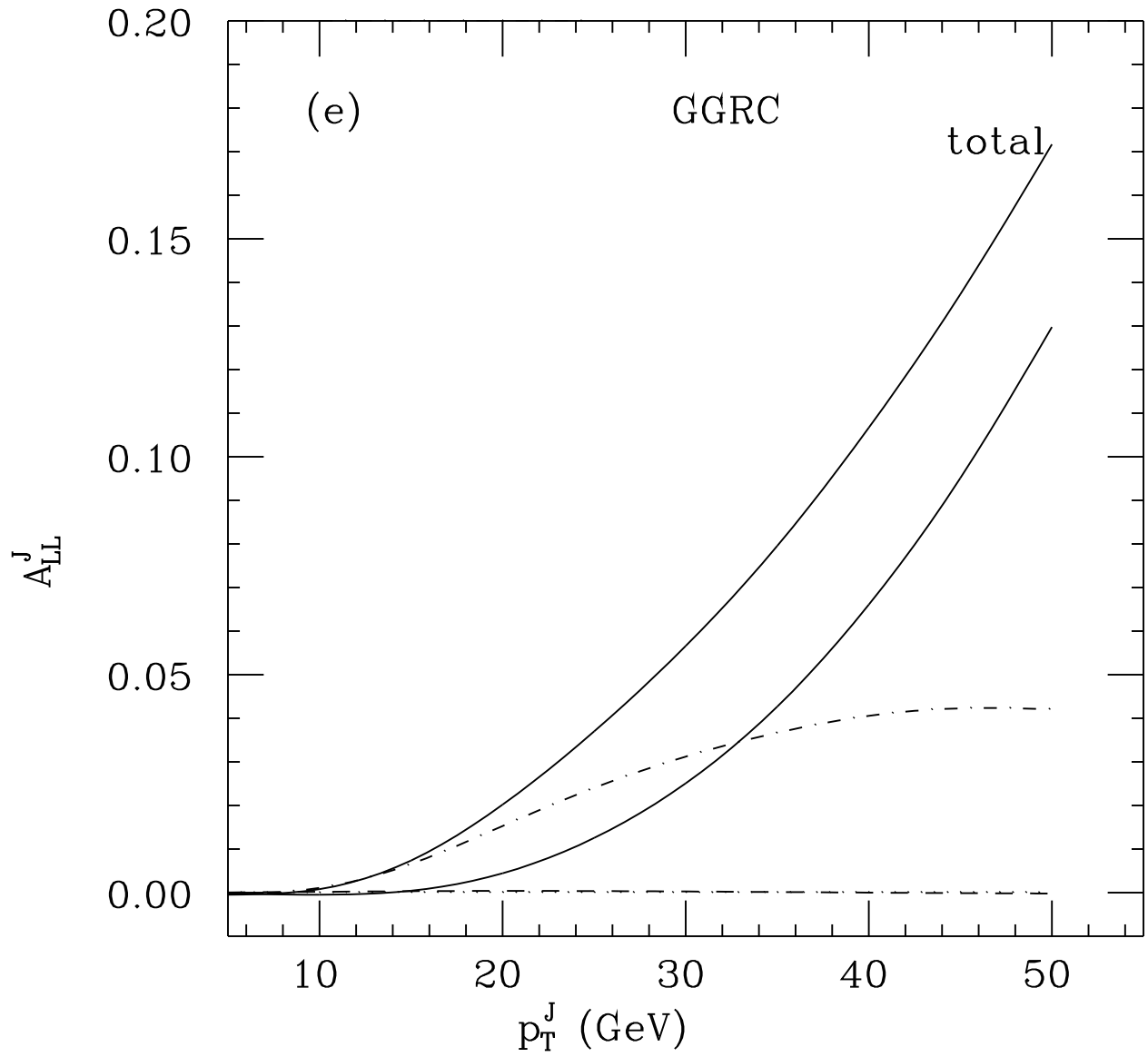


Fig. 5e



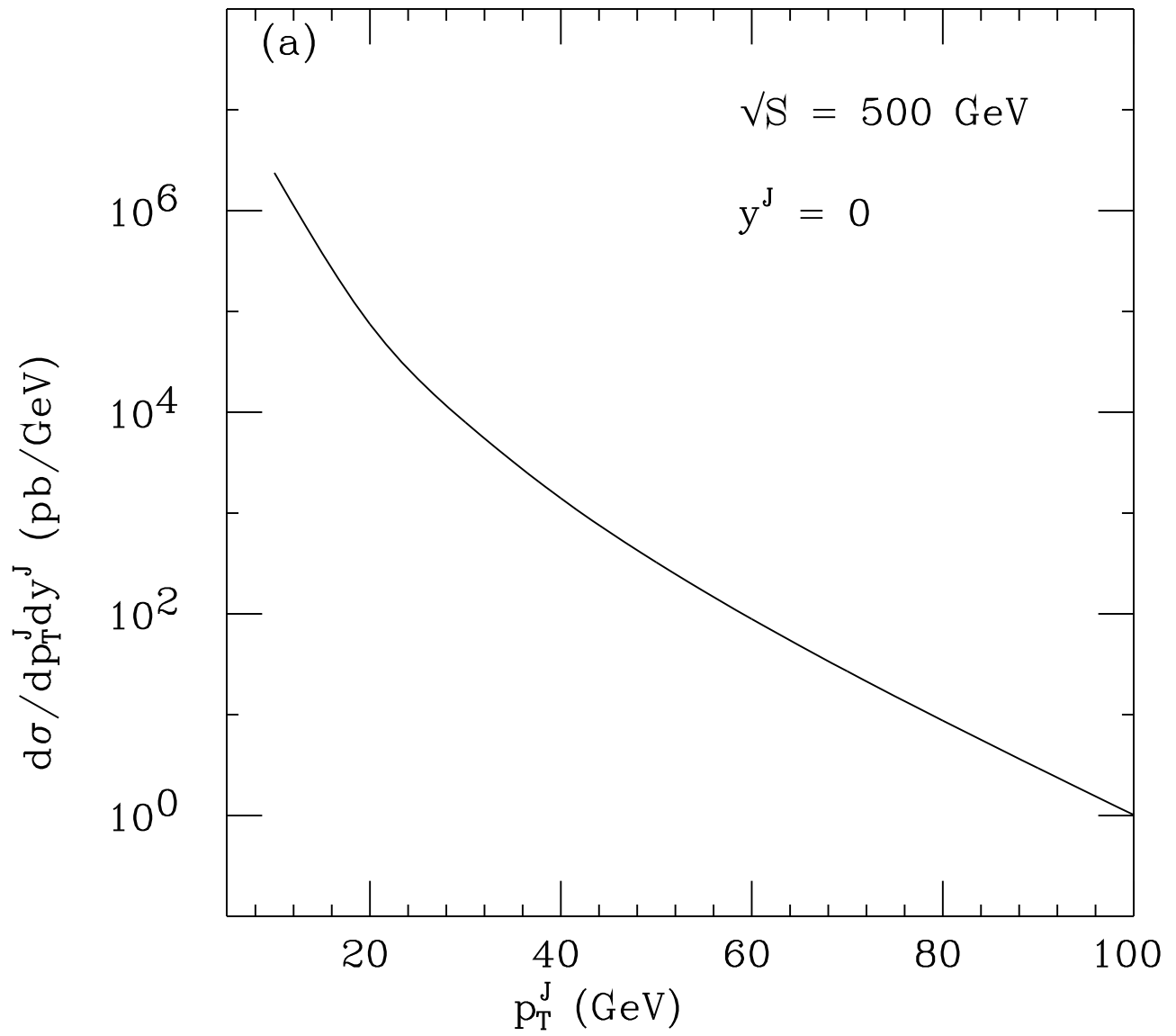


Fig. 6a

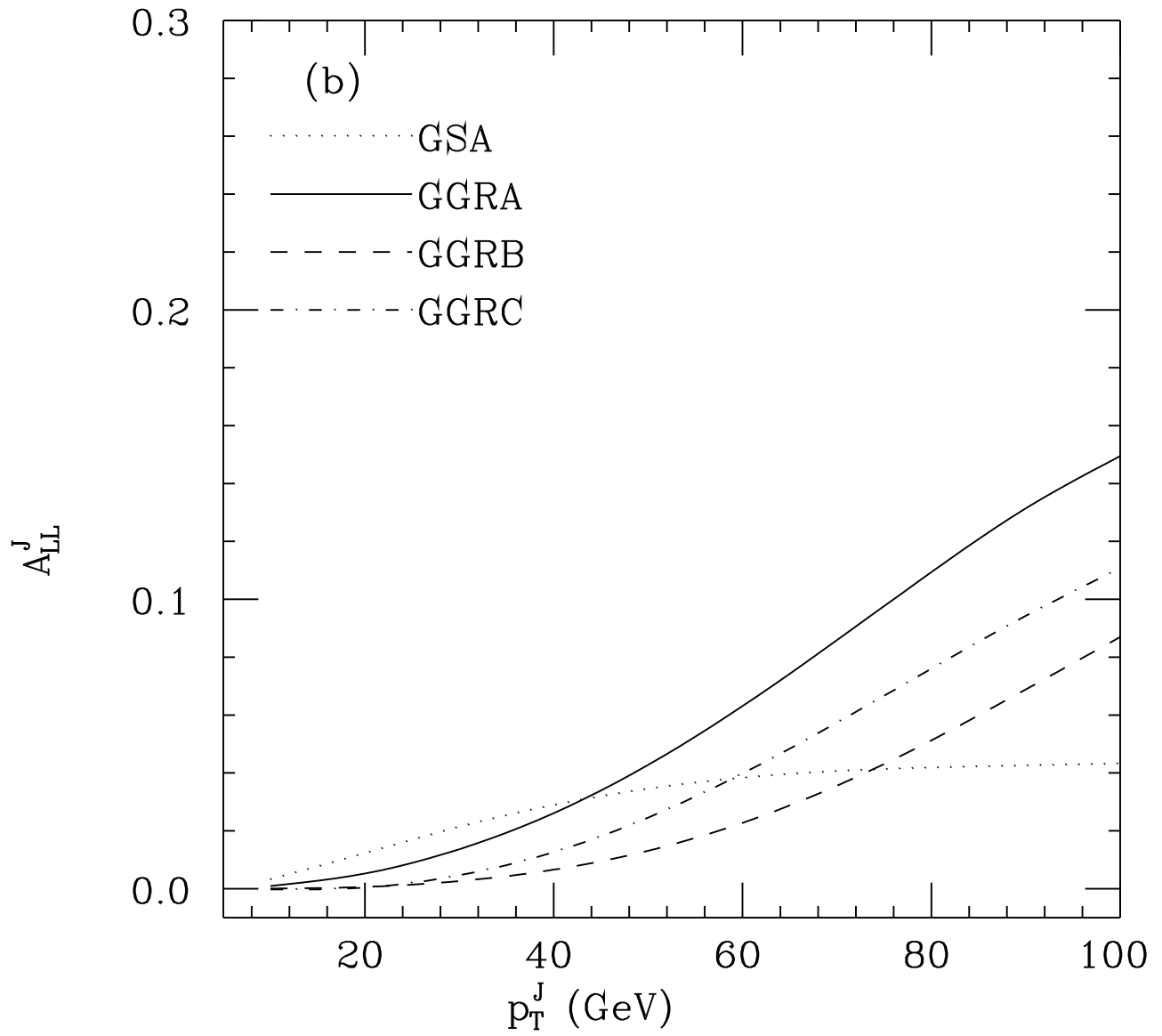


Fig. 6b